Archives of Biochemistry and Biophysics 776 (2026) 110700

Contents lists available at ScienceDirect

Archives of Biochemistry and Biophysics

journal homepage: www.elsevier.com/locate/yabbi

Adrenodoxin alters human cytochrome P450 27A1 structure and reaction efficiency beyond supplying electrons

Quoc T. Vu [a], Katherine C. May [a], Leonard B. Collins [b], Ying Xi [b], Zachary B. Davis [a], Jackson L. Bartholomew-Schoch [a], Lindsay R. Vaughn [a], Katherine R. Provost [a], Noah L. Arnold [a], Ethan F. Harris [a], Emma K. Stone [a], Hayden K. Campbell [a], Lyndsay M. Snider [a], Taufika Islam Williams [b,c], Michael J. Reddish [a,*]

[a] Department of Chemistry and Fermentation Sciences, Appalachian State University, Boone, NC, 28608, United States
[b] Molecular Education, Technology, and Research Innovation Center (METRIC), North Carolina State University, Raleigh, NC, 27695, United States
[c] Department of Chemistry, North Carolina State University, Raleigh, NC, 27695, United States

ARTICLE INFO

Keywords:
Cytochrome P450
Protein cross-linking
Mass spectrometry (MS)
Enzyme kinetics
P450 27A1
Adrenodoxin
And nano liquid chromatography (nanoLC)

ABSTRACT

Human cytochrome P450 (P450) 27A1 catalyzes the hydroxylation of cholesterol and vitamin D derivatives. P450 27A1 is localized in the mitochondria and is reduced by its redox partner protein adrenodoxin twice for each catalytic cycle. The reliance on adrenodoxin is conserved across all human mitochondrial P450 enzymes. This study examines the adrenodoxin interaction with P450 27A1 and draws comparisons with studies of other P450 enzymes to determine if differences exist. The P450-adrenodoxin complex structure was examined by chemical crosslinking and analyzed by mass spectrometry. The effect of adrenodoxin concentration on P450 27A1 function was assessed by studying effects on steady state enzyme kinetics parameters and equilibrium substrate binding. The results suggest that adrenodoxin binds to P450 27A1 at a proximal site like other P450 enzymes but differs in the specific residues involved. Furthermore, the presence of adrenodoxin and/or substrate decreases the number of interprotein and intraprotein crosslinks observed, indicating that these components change the conformation of the P450 enzyme. Increased adrenodoxin concentration causes the P450 and vitamin D_3 k_{cat} value to increase, the k_{cat}/K_m value to decrease, and the substrate K_d to remain constant. These results suggest adrenodoxin alters enzyme efficiency beyond electron transfer without affecting substrate loading. The adrenodoxin effects on P450 27A1 kinetics and equilibrium constants differ from those of other human mitochondrial P450 enzymes. In total, these structural and functional studies suggest that while the general adrenodoxin binding site and function is conserved across P450 enzymes, the details and additional effects of this interaction vary.

1. Introduction

Cytochrome P450 (P450) enzymes are a family of monooxygenase, heme-containing enzymes responsible for several important physiological reactions on both endogenous and xenobiotic substrates in many organisms. The most common reaction catalyzed by these enzymes is a carbon hydroxylation; however, heteroatom oxidations, C–C bond cleavages, and other reactions are also catalyzed by these enzymes [1,2]. In humans, there are 57 different P450 genes potentially encoding 57 different enzymes. Seven of these genes encode enzymes that become

Abbreviations: P450, cytochrome P450; Adx, adrenodoxin; AdR, adrenodoxin reductase; MS, mass spectrometry; LB, Luria-Bertani; TB, Terrific Broth; IPTG, isopropyl β-D-1-thiogalactopyranoside; DTT, dithiothreitol; CV, column volume; EDC, 1-ethyl-3-(3-dimethylaminopropyl)carbodiimide hydrochloride; ABC, ammonium bicarbonate; ACN, acetonitrile; FA, formic acid; IAA, iodoacetamide; BCA, bicinchoninic acid; *E. coli*, *Escherichia coli*; DMM, dexmedetomidine hydrochloride; P450 11A1, is enzyme commission 1.14.15.6; P450 11B1, is enzyme commission 1.14.15.4; P450 11B2, is enzyme commission 1.14.15.4; P450 24A1, is enzyme commission 1.14.15.16; P450 27A1, is enzyme commission 1.14.15.15; P450 27B1, is enzyme commission 1.14.15.18; P450 27C1, is enzyme commission 1.14.19.53; P450cam (P450 101A1), is enzyme commission 1.14.15.1; Adrenodoxin reductase, is enzyme commission number 1.18.1.6; Cytochrome P450 reductase, is enzyme commission number 1.6.2.4.

* Corresponding author.
E-mail address: reddishmj@appstate.edu (M.J. Reddish).

https://doi.org/10.1016/j.abb.2025.110700
Received 18 July 2025; Received in revised form 6 November 2025; Accepted 9 December 2025
Available online 23 December 2025

localized in the mitochondrial membrane, including P450s 11A1, 11B1, 11B2, 24A1, 27A1, 27B1, and 27C1 [3]. These mitochondrial P450 enzymes primarily interact with endogenous substrates including derivatives of steroids, secosteroids (including vitamin D), bile acids, and vitamin A [3,4].

Another distinguishing and unifying feature of the human mitochondrial P450 enzymes is their electron delivery system. Human mitochondrial P450 enzymes are considered Class I P450 enzymes, which utilize a two-protein ferredoxin and ferredoxin reductase redox system [5]. In humans, this system includes the 2Fe–2S ferredoxin known as adrenodoxin (Adx) and the FAD-dependent ferredoxin reductase known as adrenodoxin reductase (AdR). The other 50 human P450 enzymes are localized in the endoplasmic reticulum and are Class II P450 enzymes that utilize cytochrome P450 reductase [6].

Class I ferredoxin-dependent redox systems for P450 enzymes are common among bacterial P450 systems. The most well studied of these systems includes P450cam (P450 101A1). With P450cam, it has been shown that the presence of the ferredoxin protein can have effects on catalysis beyond simply supplying electrons. For example, the ferredoxin redox partner of P450cam induces major conformational changes in P450cam [7–9]. It is also suggested that the presence of the ferredoxin increases the coupling efficiency of NADH usage to P450 product formation [10]. Finally, the catalytically active, reduced oxygen-bound states of P450cam (including Compound 0 and 1) are less stable in the presence of adrenodoxin [11,12]. Given that bacterial homologues of adrenodoxin can play significant roles in catalysis other than electron delivery, it follows that adrenodoxin may also contribute beyond simple reduction in humans. Furthermore, with the key roles that the human mitochondrial P450 enzymes play in maintaining normal physiological functioning, it is important to characterize all contributions of adrenodoxin to P450 catalysis.

Multiple studies have examined the P450-adrenodoxin interaction with different human mitochondrial P450 enzymes using a variety of techniques. Studies of P450s 11B1 and 11B2 have shown that the presence of excess adrenodoxin can significantly alter both steady state k_{cat} and K_m enzyme parameters. Those same studies also show excess adrenodoxin can alter the binding of substrate to the P450 enzyme, as measured by significant changes in substrate K_d values [13,14]. In contrast, studies of P450s 11A1, 24A1, and 27C1 show that excess adrenodoxin has no effect on substrate binding [15–17]. The key protein residues driving the binding interactions of human mitochondrial P450 enzymes with adrenodoxin have also been investigated. Alterations of proposed key residues, either by chemical modification or mutation to another amino acid, have been used to investigate the roles of these residues with P450s 11A1 [18–22], 27A1 [23], and 27B1 [24]. Chemical crosslinking of a P450 enzyme to adrenodoxin followed by mass spectrometry analysis to determine interacting residues has also been used to investigate binding interactions with P450s 11B1 [25], 11B2 [25], 24A1 [26], and 27C1 [17]. Finally, single polypeptide chain fusion constructs of adrenodoxin, a peptide linker, and a P450 have been created separately with both P450s 11A1 [27] and 11B2 [14] and used in X-ray crystallography studies to explore P450 and adrenodoxin interactions. Across the investigations of key interacting residues, it appears that the overall orientation of the two proteins when interacting is consistent (adrenodoxin binds on the proximal P450 side near where the heme-ligated cysteine is), the primary driver for the interaction is electrostatic (between basic residues from the P450 and acidic residues from adrenodoxin), but the specific residues that drive this interaction can vary. From the differing impacts of adrenodoxin on P450 function and structure amongst the different P450 enzymes, it is clear that the interaction of each P450 with adrenodoxin must be studied independently.

Human cytochrome P450 27A1 is notably absent from the P450 and adrenodoxin interaction studies described above, except for the mutational studies. P450 27A1 catalyzes the oxidation of alkyl tails (the 25, 26, or 27 carbon position) of 5β-cholestane-3α,7α,12α-triol [28], lumisterol 3 [29], cholesterol [30], vitamin D_3 [30], and other similar molecules. It has also been proposed that P450 27A1 plays an important role in the oxidation of cholesterol to 27-hydroxycholesterol and the cholesterol derivative oncosterone to 27-hydroxyoncosterone. While 27-hydroxycholesterol and oncosterone were found to increase tumor growth, 27-hydroxyoncosterone was found to decrease tumor growth [31]. This suggests a complete understanding of P450 27A1 function, including the role of adrenodoxin, will impact understanding of human health in both normal and disease states. In this report, we utilize chemical crosslinking of P450 27A1 and adrenodoxin in combination with mass spectrometry (MS) analysis to investigate the nature of the binding between these two proteins. We follow that work with an investigation of the role of adrenodoxin on P450 27A1 steady state kinetics and equilibrium substrate binding.

2. Experimental procedures

2.1. Reagents

Vitamin D_3 (cholecalciferol) and calcifediol were purchased from MilliporeSigma (Burlington, MA). Solvents, buffers and other reagents required for the assays were purchased from MilliporeSigma, VWR (Radnor, PA) or Fisher Scientific (Hampton, NH) unless specifically noted.

2.2. Amino acid numbering

In this work, the amino acid numbering scheme utilized to describe adrenodoxin and cytochrome P450 residues is based on UniProt entries. Specifically, residue numbering is based on Uniprot entries: adrenodoxin - P10109, P450 27A1 - Q02318, P450 11A1 - P05108, P450 11B1 – P15538, P450 11B2 – P19099, P450 24A1 - Q07973, P450 27A1 - Q02318, P450 27B1 – O15528, and P450 27C1 - Q4G0S4. This is different than other previously published works. Numbering shifts from publication to publication based on previously reported mature protein sequences after transit peptide removal or based on recombinant sequence used. For example, Asp-77 of adrenodoxin in Ref. [17], is Asp-72 in Ref. [25] and Asp-132 in UniProt P10109. The Supporting Information provides alignments of relevant full, mature, and recombinant sequences for human adrenodoxin and human cytochrome P450 27A1. Briefly, the UniProt full sequence numbering for adrenodoxin is 60 greater than the reported mature sequence numbering; the UniProt full sequence numbering for human cytochrome P450 27A1 is 33 greater than the reported mature sequence numbering.

2.3. Recombinant protein

The plasmids for bovine adrenodoxin reductase (AdR) and human P450 27A1 production were provided as gifts from Prof. F. Peter Guengerich. The AdR pCWori$^+$ plasmid construction was described previously, and the protein expression and purification procedures were performed as described previously [32]. The P450 27A1 pCWori$^+$ plasmid construction was described previously, and the protein expression and purification procedures were performed as described previously [33]. The P450 concentration was determined prior to storage at −80 °C by measuring the reduced carbon monoxide–binding spectrum using the method of Omura and Sato with the extinction coefficient of $\epsilon_{450\ nm} = 0.091\ \mu m^{-1}\ cm^{-1}$ [34]. The pLW01 plasmid containing the human adrenodoxin (Adx) gene was a gift from Prof. Richard Auchus [25]. Human Adx was produced by transforming the plasmid into *Escherichia coli* (*E. coli*) BL21 cells. The cells were grown on Luria-Bertani (LB) agar plate with 100 μg/mL ampicillin for the selection of cells capable of producing Adx. A colony was inoculated into 50 mL of autoclaved LB liquid media with 100 μg/mL ampicillin and incubated overnight at 37 °C and 180 rpm. Thompson (Carlsbad, CA) Ultra Yield (2.5 L size) flasks containing 500 mL Terrific Broth (TB) media with 100

μg/mL ampicillin were inoculated with 1 % (v/v) *E. coli* overnight culture prepared above. The inoculated TB media was incubated at 37 °C and 200 rpm (1-inch orbit) until the optical density reached 0.6, at which point isopropyl β-D-1-thiogalactopyranoside (IPTG) was added to a 1 mM final concentration. The TB media was then incubated at 26 °C and 150 rpm for 24 h. The cultures were then centrifuged (4000×*g*, 4 °C) for 20 min, supernatant decanted, and the pelleted cells were transferred into a metal beaker with 60 mL of sonication buffer added (100 mM potassium phosphate (pH 7.4), 20 % glycerol (v/v), 0.1 mM dithiothreitol (DTT)). The cells were lysed by sonication using a Qsonica (Newtown CT) Q700 Sonicator with a ½" diameter probe (#4220) set at 70 % amplitude for 6 rounds of 30 s on and 30 s off while on ice. The sonicated cells were then centrifuged (100,000×*g*, 4 °C) for 1 h. The supernatant was transferred to 50 mL conical tubes, after which 20 mM of imidazole was added to the supernatant. An Äkta start FPLC system (Cytiva, Wilmington, DE) was prepared with a prepacked Ni-NTA-agarose column (Cytiva HisTrap HP, 5 mL column volume (CV)). The column was equilibrated with buffer A (20 % glycerol (v/v), 50 mM potassium phosphate (pH 7.4), and 0.1 mM DTT) at 5 mL/min for 10 column volumes (CV). The Adx-containing supernatant was then loaded into the column at 1 mL/min. The column was then washed with buffer A with 10 mM imidazole, washed again with buffer A with 25 mM imidazole, and eluted with buffer C with 250 mM imidazole. The wash and elution phases were 10 CV in length and at a flow rate of 2 mL/min. The protein fractions were visualized with sodium dodecyl sulfate polyacrylamide gel electrophoresis (SDS-PAGE). The fractions showing Adx presence were combined, placed in Thermo Scientific SnakeSkin dialysis tubing with a 3500 Da molecular weight cutoff, and dialyzed against buffer B (20 % glycerol (v/v), 100 mM potassium phosphate pH 7.4) twice for 24 h each time. The final Adx concentration was measured using ultraviolet–visible spectroscopy with Adx absorbance at 414 nm and the extinction coefficient of 9800 $M^{-1}cm^{-1}$ [35].

2.4. Chemical crosslinking

For crosslinking studies, aliquots of human P450 27A1 and human Adx were removed from a −80 °C freezer and thawed on ice. Two solutions were prepared for overnight dialysis at 4 °C to remove glycerol in Thermo Scientific (Waltham, MA) G3 Slide-a-lyzer cassettes with a 10,000 Da molecular weight cutoff. Solution One contained only P450 27A1 and was dialyzed against 100 mM potassium phosphate (pH = 7.4). Solution Two contained P450 27A1 and Adx and was dialyzed against 10 mM potassium phosphate (pH = 7.4). The lower concentration of potassium phosphate was used for the two-protein solution as lower ionic strength favors P450-Adx complex formation; however, a higher potassium phosphate concentration was required when P450 27A1 was alone to prevent protein aggregation [25,26]. Solutions were checked for dilution the next morning by comparing UV–Vis absorption spectra to spectra recorded the previous day. A fresh solution of vitamin D_3 was prepared in 90 % ethanol with 10 % ultrapure water (H_2O), and its concentration was confirmed by UV–Vis absorbance spectroscopy at 265 nm using an extinction coefficient of 18,300 $M^{-1}cm^{-1}$ [36,37]. A fresh solution of the crosslinking reagent 1-ethyl-3-(3-dimethylaminopropyl)carbodiimide hydrochloride (EDC) was prepared in ultrapure H_2O. Three replicates of six different sample types were prepared for crosslinking. See Table 1 for sample type composition. No samples contained detergent during dialysis or crosslinking steps to match conditions of studies with other mitochondrial P450 enzymes [17,25,26]. After separately mixing all samples, they were incubated at 25 °C while shaking at 300 rpm in an Eppendorf (Hamburg, Germany) New Brunswick Innova 42R refrigerated shaker incubator with a 1" orbit. After approximately 3 h of crosslinking time, the crosslinking reaction was stopped.

The small and large volume sample types were processed differently after completion of the crosslinking reaction. For sample types 1–4 that were originally 140 μL, the crosslinking reaction was stopped by the addition of 49.3 μL of lithium dodecyl sulfate sample buffer (4X) from GenScript (Piscataway, NJ) and 7.89 μL of 2.5 M DTT (final concentration of DTT was 100 mM). These sample were then heated at 80 °C for 15 min, centrifuged briefly, and further purified by SDS-PAGE electrophoresis After staining, gel bands representing each of the protein or protein complexes to be examined were excised with a razor blade, cut unto small cubes, flash frozen in liquid nitrogen, and stored at −80 °C prior to shipment to the Molecular Education, Technology and Research Innovation Center (METRIC) at NC State University for mass spectrometry analysis. For sample types 5–6, the crosslinking reaction was stopped by passing each sample through its own Thermo Zeba spin desalting column, flash freezing the sample in liquid nitrogen, and storing the sample at −80 °C prior to shipment to METRIC. Additional sample preparation details are provided in the Supporting Information.

2.5. Mass spectrometric sample preparation, analysis, and data treatment

Sample types 1–4 (gel samples) were processed at METRIC through a series of steps to remove gel stain, reduce disulfide bonds with DTT, alkylate sulfur groups, digest proteins with trypsin, dry sample for storage, and then reconstitute the day of analysis in 98 : 2: 0.1H_2O: acetonitrile: formic acid. Sample types 5–6 (liquid samples) were processed to achieve similar results but without the destain step. The amount of liquid sample to process was determined by bicinchoninic acid (BCA) assay analysis to achieve 200 μg of protein in the sample. Additional sample preparation details are available in the Supporting Information.

Prepared samples were loaded onto a Thermo Fisher Scientific Vanquish NEO UHPLC system (Germering, Germany) for in-line trap-and-elute, followed by analytical column separation of tryptic peptides.

Table 1
Composition of crosslinking sample types and their usage.

Sample Type	Sample Usage	Sample Volume	[P450 27A1]	[Vitamin D_3]	[Adrenodoxin]	[EDC]	Final Buffer Composition
1	SDS-PAGE Gel Separated for Intraprotein Crosslinks Analysis	140 μL	2 μM	–	–	2 mM	99 mM Potassium Phosphate (pH = 7.4)
2[a]	SDS-PAGE Gel Separated for Intraprotein Crosslinks Analysis	140 μL	2 μM	40 μM	–	2 mM	99 mM Potassium Phosphate (pH = 7.4), 0.49 % ethanol
3	SDS-PAGE Gel Separated for Intraprotein Crosslinks Analysis	140 μL	2 μM	–	40 μM	2 mM	10 mM Potassium Phosphate (pH = 7.4)
4[a]	SDS-PAGE Gel Separated for Intraprotein Crosslinks Analysis	140 μL	2 μM	40 μM	40 μM	2 mM	10 mM Potassium Phosphate (pH = 7.4), 0.49 % ethanol
5	Solution Sample for Interprotein Crosslinks	950 μL	2 μM	–	40 μM	2 mM	10 mM Potassium Phosphate (pH = 7.4), 0.49 % ethanol
6[a]	Solution Sample for Interprotein Crosslinks	950 μL	2 μM	40 μM	40 μM	2 mM	10 mM Potassium Phosphate (pH = 7.4), 0.49 % ethanol

[a] Samples containing vitamin D_3 had a final organic solvent content of 0.49 % ethanol (v/v). This solvent content was not compensated for in samples without vitamin D_3. The small amount of ethanol present with substrate was not considered to be significant and was not compensated for in samples without substrate.

The sample was first passed through a Thermo Scientific 0.5 cm length (300 μm inner diameter, 5 μm particle size) octadecylsilane (C18) reversed phase trap column (Fisher Catalog # 174500) for concentration and washing. The sample was then passed through a Thermo Scientific 50 cm (75 μm inner diameter, 2 μm particle size) C18 reversed phase analytical column (Fisher Catalog # ES75500PN). The mobile phase solvents were (solvent A) 98 % H_2O, 2 % ACN, 0.1 % FA and (solvent B) 80 % ACN, 20 % H_2O, 0.1 % FA (all v/v). The elution gradient was 0–1 min. 2 % B, 1–3 min. 2–10 % B, and 3–93 min. 10–75 % B followed by a column wash from 93 to 98 min at 75–95 % B and from 98 to 106 min at 95 % B, all at a flow rate of 0.30 μL/min. A Thermo Scientific Orbitrap Eclipse Tribrid MS (San Jose, CA, USA) with EASY-Spray source was used in positive ion mode for full MS/data-dependent analysis or DDA MS/MS (top speed) analysis. The full MS settings were microscans: 1, orbitrap resolution: 120,000, AGC target: Custom, Normalized AGC Target (%): 250, maximum injection time: 50 ms, and scan range: 375-1500 *m/z*. The DDA settings were microscans: 1, resolution: 15,000, AGC Target: Custom, Normalized AGC Target (%): 100, maximum injection time: Auto, isolation window: 1.6 *m/z*, and Scan Range Mode: Auto.

Proteome Discoverer (PD) version 2.5.0.400) was used for database and crosslink searching. The search database consisted of the *Escherichia coli* proteome and the human adrenodoxin and cytochrome P450 27A1 recombinant sequences. Any mass spectra result that was not identified in the database was analyzed by the XLinkX node in PD to search against the recombinant protein sequences with crosslink modification present [38]. Additional details, including software parameters, are available in the Supporting Information. The data presented in the Results section indicates the number of times a particular crosslink was identified across the three sample type replicates (not instrument injection replicates) with a Max XLinkX score of 20 or greater. In some cases, a precursor MS1 peak of a crosslink was found in a sample, but the precursor signal was too low to obtain a confirmatory MS2 spectrum. In these cases, a sample was considered to not have the crosslink due to low signal. Therefore, the data presented here are of high confidence, but may be under-reporting some crosslinks. Tables of crosslinked peptides recognized by XLinkX and details on the MS data leading to those assignments is available in a separate Microsoft Excel file as Supporting Information.

2.6. Molecular modeling

To aid in the interpretation of crosslinking data, a molecular docking approach was taken. The experimental X-ray crystal structure of human adrenodoxin was obtained from the Protein Data Bank (PDB ID: 3P1M) [39]. Chain G was isolated from the rest of the structure into a new PDB file and used for modeling. There was no publicly available experimental structure of human P450 27A1 at the time of analysis. Instead, a structure was predicted using the recombinant protein sequence as an input in AlphaFold2 managed by the ColabFold platform in the ChimeraX software [40–43].

Docking of the two proteins was performed in three steps. In step one, the DisVis software and web server were used to determine which groups of crosslinked residues found in the mass spectrometry data could be used as constraints together and lead to protein configurations where all restraints were simultaneously fulfilled [44–46]. In the second step of molecular modeling, the mixture of restraint subsets that could be fulfilled simultaneously were analyzed again by DisVis to determine the likely accessible interaction space between P450 27A1 and adrenodoxin. In the third step of molecular modeling, the HADDOCK 2.4 software and web server were used to predict the structure of P450-adrenodoxin complexes based on the restraints sets derived in the previous two steps [46,47]. Additional details for these steps, including software settings, can be found in the Supporting Information.

2.7. Steady state kinetics

The steady state kinetics of the human cytochrome P450 27A1 catalyzed transformation of vitamin D_3 into 25-hydroxyvitamin D_3 (calcifediol, 25(OH)D_3) were examined with human Adx as the redox partner. Reactions (final volume of 500 μL) were carried out in 10 mL glass test tubes, containing 0.2 μM P450 27A1, 0.2 μM bovine AdR, in 50 mM potassium phosphate buffer (pH 7.4), and with various vitamin D_3 concentrations (1, 4, 5, 7, 10, 15, 20, 25, 30, 35, 50 μM). Human Adx was added to a final concentration of 0.2 μM human Adx (for 1:1 Adx:P450 27A1) or 0.6, 2, 10 μM (for 3:1, 10:1, 50:1 Adx:P450 27A1, respectively). Prior to the addition, vitamin D_3 solutions were prepared fresh daily in 90 % ethanol (v/v). Triplicates of each reaction were preincubated in a 37 °C shaking water bath for 5 min, after which NADPH was added to the tubes with a final concentration of 1 mM to initiate the reaction. The reactions were allowed to proceed at 37 °C, stopped by adding 2 mL of pure ethyl acetate, and mixed by vortex. Reactions with 0.2 μM human Adx were stopped after 15 min. Reactions with 0.6, 2, or 10 μM human Adx were stopped after 7 min. The tubes were centrifuged (2000×*g*) for 2 min to separate the aqueous and organic layer. Next, the organic layers containing vitamin D_3 and calcifediol were extracted (1.5 mL) into new glass tubes, which were then evaporated under nitrogen stream for 30 min. The dried organic layers were resuspended with 250 μL of 50:50 acetonitrile:water (ACN:H_2O, v/v). The mixtures were transferred to 2 mL amber glass vials with Fisher Scientific Fisherbrand 350 μL glass autosampler vial inserts. The resulting samples were analyzed using a 1260 Infinity II LC system (Agilent, CA) with a photodiode array detector for absorbance measurements. Aliquots of samples (25 μL) were injected on a Thermo Fisher Scientific Accucore C18 column (2.6 μm particle size, 30 × 2.1 mm). Mobile phase A was 95 % H_2O, 5 % ACN, and 0.1 % formic acid (all v/v). Mobile phase B was 100 % ACN, and 0.1 % formic acid (all v/v). The flow rate of the mobile phase was 0.35 mL/min, and the elution gradient was as follows: 0–2 min 50 % B, 2–7 min 50–100 % B, 7–10 min 100 % B; 10–10.5 min 100-50 % B, and 10–13 min 50 % B. The column temperature was 25 °C and the absorbance was measured at 265 nm. The identities of vitamin D_3 and calcifediol were determined by retention time comparisons to authentic standards. The resulting chromatogram peak areas of calcifediol were analyzed using Agilent OpenLab software. Peak areas were adjusted for liquid dilutions and concentrations in the sample workup process. The calcifediol concentrations were determined by comparison to a set of external calibrants of known concentrations made fresh and tested for each experiment (0.02, 0.05, 0.1, 0.2, 0.5, 1, 2 μM). Product concentrations were converted to product rates and analyzed in GraphPad Prism software version 10.4.1 (GraphPad, San Diego, CA). The steady state kinetics parameters k_{cat} and k_{cat}/K_m (represented here as k_{sp}) were fit directly by nonlinear hyperbolic regression using a custom formula in the same program; K_m was then derived from the values of k_{cat} and k_{cat}/K_m. Direct fitting of k_{cat} and k_{cat}/K_m has advantages over the tradition fitting of k_{cat} and K_m, including reducing errors in fitting. These advantages are discussed more thoroughly in Ref. [48]. The formula used for fitting is shown in Equation (1) where k_{sp} is equivalent to k_{cat}/K_m.

$$v = \frac{k_{sp} \cdot [Substrate]}{1 + \frac{k_{sp} \cdot [Substrate]}{k_{cat}}} \quad \text{(Eq. 1)}$$

2.8. Equilibrium substrate binding

The equilibrium dissociation constants of vitamin D_3 (K_{dVD3}) to P450 27A1 were determined spectrophotometrically at various concentrations of Adx. These experiments had to be performed as a competition experiment since vitamin D_3 did not induce a spectral change in P450 27A1 by itself. The competing ligand used was dexmedetomidine hydrochloride (DMM), a known inhibitor of human P450 27A1 [49]. The binding affinity of DMM for P450 27A1 was measured with and without

vitamin D_3 to determine both the apparent equilibrium inhibitor dissociation constant ($K_{dDMMapp}$) and the equilibrium inhibitor dissociation constant (K_{dDMM}), respectively, which were used to calculate K_{dVD3}, at a given concentration of vitamin D_3. Equation (2) describes the direct competition relationship between vitamin D_3 and DMM assuming no allosteric binding [50].

$$K_{dVD3} = \frac{[Vit\ D_3]}{\left(\frac{K_{dDMMapp}}{K_{dDMM}}\right) - 1} \quad \text{(Eq. 2)}$$

For the titration of DMM without vitamin D_3, a 2 mL solution of 1 μM P450 27A1, 1 μM Adx (for 1:1 Adx:P450 27A1) or 3, 10, 50 μM (for 3:1, 10:1, 50:1 Adx:P450 27A1, respectively), 50 mM potassium phosphate buffer (pH 7.4) was prepared, split equally between two 1 cm cuvette cells (FireflySci, Brooklyn, NY, product number 9UV10-2 EA), and scanned for an absorbance spectrum in a Shimadzu UV-2600 double-beam ultraviolet–visible spectrophotometer (Shimadzu Scientific, Kyoto, Japan) from 350 to 500 nm. Small volumes of DMM stock solutions (0.5–7 mM) in 90 % ethanol were titrated into the titrant cell (ethanol final concentration <1.5 % (v/v)), while the reference cell was titrated with the same volume of the solvent used to make DMM stock solutions. The cells were mixed gently after each addition by pipetting the solution up and down with a micropipette several times. A difference spectrum of the sample and reference cells was generated by the subtraction between the absorbances of the cell with DMM as titrant minus the absorbances of the reference cell. The differences between the absorbances of the maximum (typically 434 nm) and minimum (typically 413 nm) of the difference spectrum were plotted against the total DMM concentrations in the titrant cell. For the titration of DMM with vitamin D_3, the procedures were the same as the titration without vitamin D_3, except the addition of 1 μM vitamin D_3 in the 2 mL P450 27A1 solution prior to titration. The K_{dDMM} and $K_{dDMMapp}$ were measured by fitting the differences in maximum and minimum intensity versus concentration of DMM using nonlinear regression to a quadratic binding equation in the Prism software. Equation (3) describes this nonlinear fitting, where y is the spectral difference; y_o is spurious background spectral signal; A is the spectral coefficient; E is the total enzyme concentration; K_{dDMM} is the K_d of DMM (or $K_{dDMMapp}$, for titration with vitamin D_3), and x is the total titrant concentration. The real value of the vitamin D_3 K_d (K_{dVD3}) was then calculated assuming direct competition between DMM and vitamin D_3 using Equation (2) described above.

$$y = y_o + \left(\frac{A}{2 \cdot E}\right) \cdot \left((K_{dDMM} + E + x) - \sqrt{(K_{dDMM} + E + x)^2 - (4 \cdot E \cdot x)} \right) \quad \text{(Eq. 3)}$$

Additionally, in GraphPad Prism software version 10.4.1, one-way ANOVA was used to determine the statistical significance ($\alpha = 0.01$) of changes in the obtained K_d values.

3. Results

3.1. Evaluation of P450-Adx interaction interface

To determine the orientation and key interacting residues when human P450 27A1 and human adrenodoxin form a complex, chemical crosslinking was performed with the proteins using the zero-length crosslinker EDC. Fig. 1 shows an example of SDS-PAGE separated crosslinking samples. In lanes 1 and 2, only bands from P450 27A1 are present. The expected recombinant molecular weight of P450 27A1 is 57.6 kDa, which is the molecular weight of the primary band present (arrow B). Bands at higher molecular weight in these lanes are likely from higher order protein aggregates. The presence of vitamin D_3 substrate in lane 2 samples during crosslinking does not appear to alter the crosslinking result by SDS-PAGE analysis. In lanes 3 and 4 SDS-PAGE bands from adrenodoxin are also present. Monomeric adrenodoxin is present around 15 kDa (arrow D, expected recombinant molecular weight is 14.5 kDa). Dimeric adrenodoxin stabilized by EDC crosslinking appears around 35 kDa (arrow C). P450-adrenodoxin crosslinked complexes in a 1:1 stoichiometry appear around 70 kDa (arrow A). Additional unidentified bands are present around 100 kDa that may represent P450-adrenodoxin complexes with more than two protein molecules present. For LC-MS/MS analysis of intraprotein crosslinks, bands were extracted from SDS-PAGE gels at the positions indicated by the arrows in Fig. 1. Fig. S1 in the Supporting Information shows an additional SDS-PAGE result comparing isolated proteins and protein mixtures with and without EDC present. The results from Fig. S1 were used to distinguish which SDS-PAGE bands are from crosslinking and which are from background sample contaminants. The combination of SDS-PAGE results from Fig. 1 and Fig. S1 suggest that EDC can be used to link P450 27A1 and adrenodoxin together in a manner that is at least resistant to heating and SDS-induced denaturation.

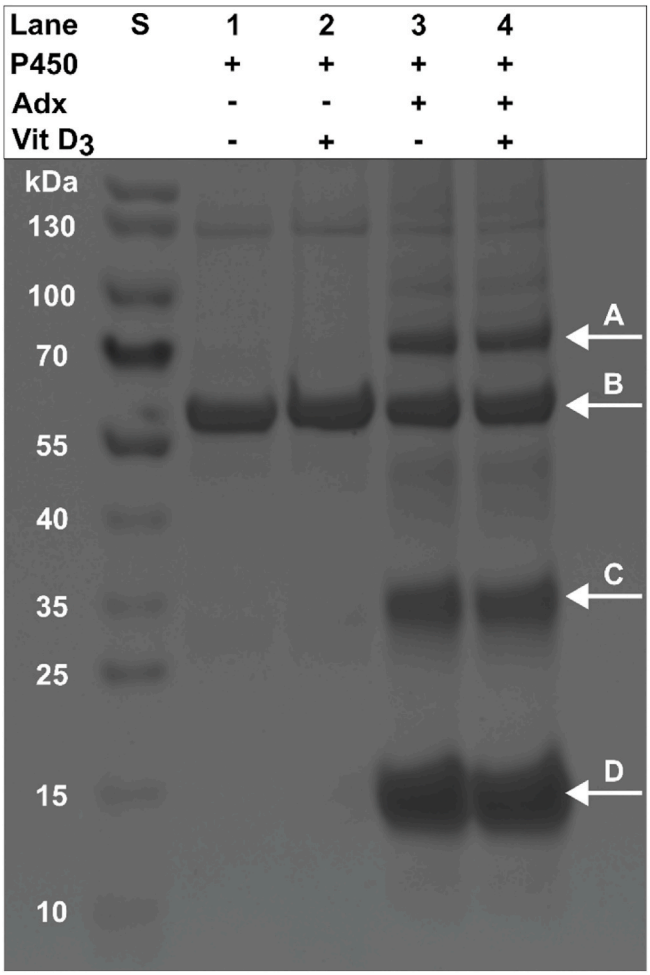

Fig. 1. Example SDS-PAGE separation of sample types 1–4 after crosslinking reaction. Lane S shows molecular weight standards. Lanes 1 and 2 show P450 mixed with the crosslinker EDC without and with vitamin D_3 present. Lanes 3 and 4 show P450 and adrenodoxin mixed with EDC without and with vitamin D_3 present. The labeled arrows A, B, and D indicate the protein bands that were removed for analysis by mass spectrometry. Arrow A indicates the P450-adrenodoxin complex band around 70 kDa. Arrow B indicates the P450 monomer band around 60 kDa. Arrow D indicates the Adx monomer band around 15 kDa. Arrow C indicates the dimeric adrenodoxin complex discussed in the text. This band was not analyzed by mass spectrometry.

Protein complexes produced by EDC crosslinking were then digested by trypsin and analyzed by LC-MS/MS to determine crosslinked residues between the two proteins. For analysis of these interprotein interactions, protein complexes were isolated from solution for analysis (i.e., not

subjected to SDS-PAGE) to increase assay sensitivity. Raw data and Proteome Discoverer data files are available on online on the website PanoramaWeb under the NCSU – METRIC Public Data repository (https://panoramaweb.org/NCSU%20-%20METRIC/project-begin.view). Detailed tables of MS data on crosslinked peptides identified by XLinkX are provided as a separate Microsoft Excel file. Fig. 2 shows example MS/MS spectra of identified interprotein crosslinks. Table 2 summarizes all the identified crosslinks with and without the P450 substrate vitamin D_3 present.

Several EDC crosslinked residues were identified. EDC crosslinks carboxylic acid groups with nearby amine groups to form a stable covalent bond. This occurs by the EDC carbodiimide activating the carboxylic acid to a o-acylisourea ester that is displaced by a primary amine group. Due to the instability of the o-acylisourea ester, only amine groups in close proximity have time to react before the o-acylisourea is degraded by hydrolysis. Only lysine amine groups are reactive under these conditions. Arginine amine group that participate in salt bridges will be missed by this technique. Other amino acid residues will not react even if they are nearby. As expected, the crosslinked residues from P450 27A1 were primarily basic residues (lysines), and the crosslinked residues from the adrenodoxin were primarily acidic residues (aspartic and glutamic acids). In samples without the substrate vitamin D_3, 13 distinct crosslinks were identified. In samples with vitamin D_3 present, only 7 distinct crosslinks were identified. All 7 of the crosslinks identified when vitamin D_3 is present were also identified when vitamin D_3 was not present. Therefore, the presence, and presumably the binding, of vitamin D_3 limits the number of ways in which the two proteins interact with one another. Vitamin D_3 could also be limiting the accessibility of

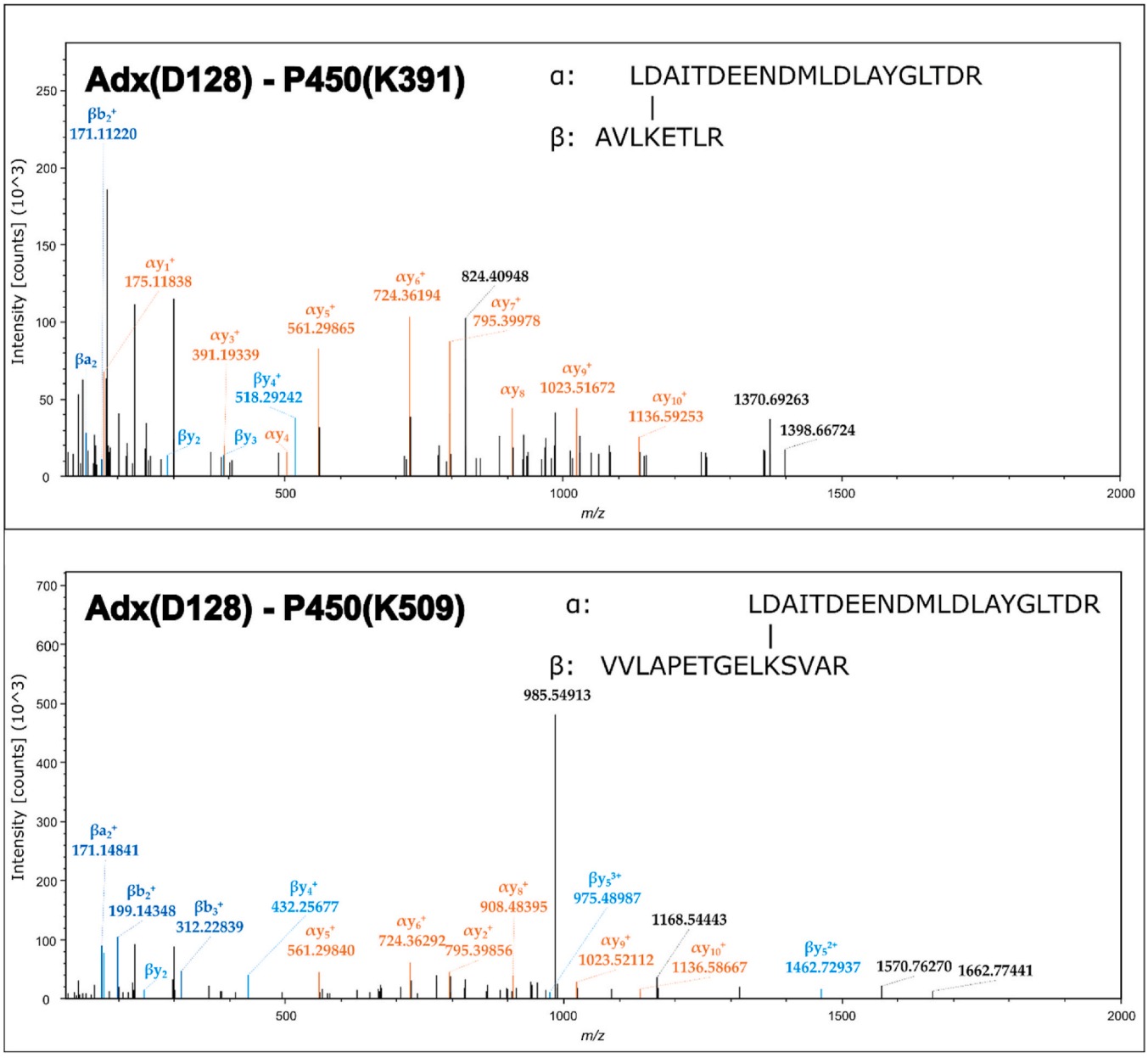

Fig. 2. Example MS/MS spectra of two identified interprotein crosslinks. The residues crosslinked and the protein of origin are shown in the top left of each spectrum. The isolated peptides containing the crosslinked residues are shown in the top right of each spectrum. Both of these spectra were obtained from sample A5. Peak colors correspond to identity assigned to peak: black – unassigned, red – a/b type ions assigned to peptide α, orange – y type ions assigned to peptide α, dark blue – a/b type ions assigned to peptide β, and light blue – y type ions assigned to peptide β. (For interpretation of the references to color in this figure legend, the reader is referred to the Web version of this article.)

Table 2
P450 27A1-Adrenodoxin (Adx) crosslinks identified with and without vitamin D_3 present.

Assigned Cluster Group	P450 Linked Residue[a]	Adx Linked Residue[b]	P450 + Adx Samples Containing the Crosslink (Out of 3)[c]	P450 + Adx + Vitamin D_3 Samples Containing the Crosslink (Out of 3)[c]
2	K39	D75	2	2
2	K39	E169	1	1
2	K39	D173	1	1
2	E58	K82	1	
1	K391	D128	1	
2	K409	D173	2	2
2	E412	K182	1	
2	D414	K182	1	1
3	K509	D128	1	1
3	K509	D132	1	
3	K520	D75	1	
3	K520	E169	1	
3	K521	D75	2	3

[a] Numbering for human P450 27A1 based on Uniprot Accession Q02318.
[b] Numbering for human adrenodoxin based on Uniprot Accession P10109.
[c] Three crosslinking samples were prepared in parallel from the same protein stocks at the same time and kept separate during workup and analysis.

certain residues to EDC. The observed crosslinking sites are far from the vitamin D_3 binding site at the heme, making the vitamin D_3 effect likely allosteric in nature and due to protein conformational changes.

The residues identified from P450 27A1 were located in three clusters. Cluster 1 includes K391 and is located on the proximal side of the P450 where adrenodoxin is expected to bind based on comparison to X-ray diffraction data of P450-adrenodoxin fusion constructs with P450 11A1 and 11B2 (PDB entries 3N9Y and 7M8I) [14,27]. K391 is between β-sheet 1 and β-sheet 2 of the P450 27A1 model predicted from AlphaFold. Cluster 2 includes K39, E58, K409, E412, and D414 and is located on the proximal side of the P450 but further away from the expected adrenodoxin binding site. When mapped to the AlphaFold prediction of P450 27A1, cluster 2 includes residues in an unstructured N-terminal region as well as β-sheet 2. Cluster 3 includes K509, K520, and K521 and is located on the distal side of the P450 near β-sheet 4, indicating a binding site unlikely to directly contribute to electron transfer. These clusters are highlighted in Fig. 3A.

The residues identified in crosslinks originating from the adrenodoxin are dispersed throughout the protein structure when compared to X-ray crystallography data from both adrenodoxin alone (PDB: 3P1M) and P450-adrenodoxin fusion constructs including P450 11A1 or P450 11B2 [14,27]. Fig. 3B displays the location of residues identified in crosslinks from adrenodoxin. Based on comparisons to fusion construct data, only D132 of human adrenodoxin appears to be positioned to form a relevant contact with the P450. Not all residues observed in our crosslinking data for adrenodoxin are resolved in the structural data of the fusion proteins. Additionally, the crystal structure data only capture a single view of the orientation and may not fully represent the conformational space of the interaction. In total, the broad spacing of crosslinked residues across the structures of both the P450 and adrenodoxin suggests that crosslinked residues likely identify multiple interaction modes.

3.2. Identification of P450–P450 intraprotein crosslinks

Chemical crosslinking of proteins and mass spectrometry analysis were also performed to analyze intraprotein crosslinks of P450 27A1 and adrenodoxin. These experiments explore how the structure of the P450 or adrenodoxin change when the proteins are isolated compared to when they are in complex with one another or with the vitamin D_3 substrate. Unlike in the interprotein crosslink analysis above performed in solution, the intraprotein crosslinks were created in solution and then purified by SDS-PAGE to make sure only the relevant protein or protein complex was being examined. If the intraprotein crosslinks had been analyzed directly from solution samples, it would have been difficult to distinguish identified P450–P450 crosslinks as an intraprotein crosslink coming from monomeric P450 vs interprotein crosslinks coming from a P450 multimer. Similar reasoning also applies to adrenodoxin intraprotein crosslinks. The top spectrum of Fig. 4 shows an example of a P450–P450 intraprotein crosslink. Table 3 lists all the intraprotein crosslinks identified in P450 27A1 under various conditions. Fig. 5A shows the location of the residues identified from P450 27A1 intraprotein crosslinking analysis modeled on an AlphaFold2 generated structure of the protein.

Five distinct EDC crosslinks are identified with isolated P450 27A1 distributed at various places on the P450 structure. One of the crosslinks shows up twice with different trypsin cleavage products attached. Two of those original five crosslinks are again identified when either adrenodoxin or vitamin D_3 is added to the reaction mixture. When both adrenodoxin and vitamin D_3 are added to the reaction mixture, a third crosslink from the original five is identified. The two crosslinks identified when either adrenodoxin or vitamin D_3 are added to the reaction mixture would map between the B and C α-helices (D129-K123) and

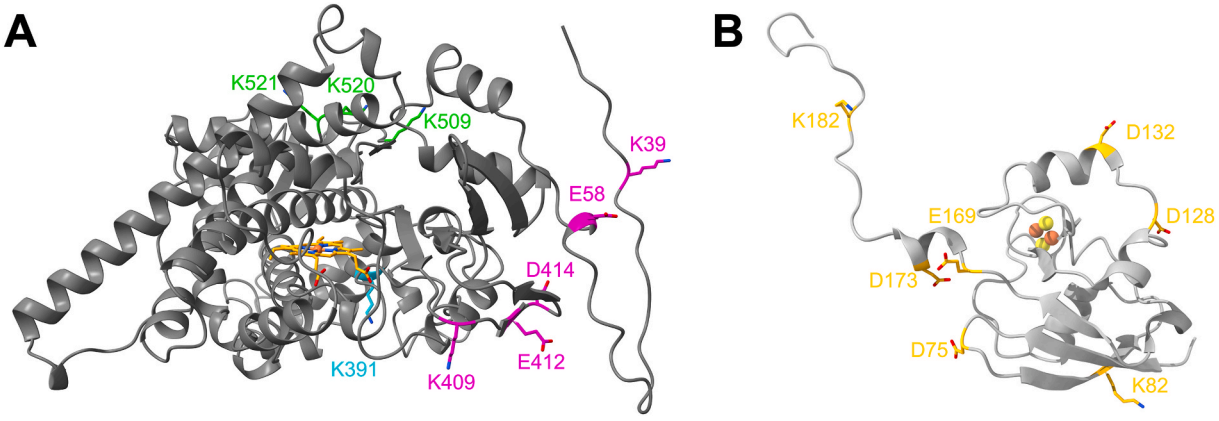

Fig. 3. A. AlphaFold-generated structure of recombinant human P450 27A1. Highlighted as stick drawings in cyan, magenta, and green are clusters 1, 2, and 3 (respectively) of residues identified from interprotein crosslinking analysis. In orange is the approximate position of the heme group as expected from comparison to PDB entry 3N9Y of a P450 11A1-adrenodoxin fusion construct. B. Adrenodoxin structure (PDB: 3P1M). Residues identified in interprotein crosslinking analysis are shown in gold as stick drawings. The 2Fe–2S cluster of adrenodoxin is shown as yellow and orange spheres. (For interpretation of the references to color in this figure legend, the reader is referred to the Web version of this article.)

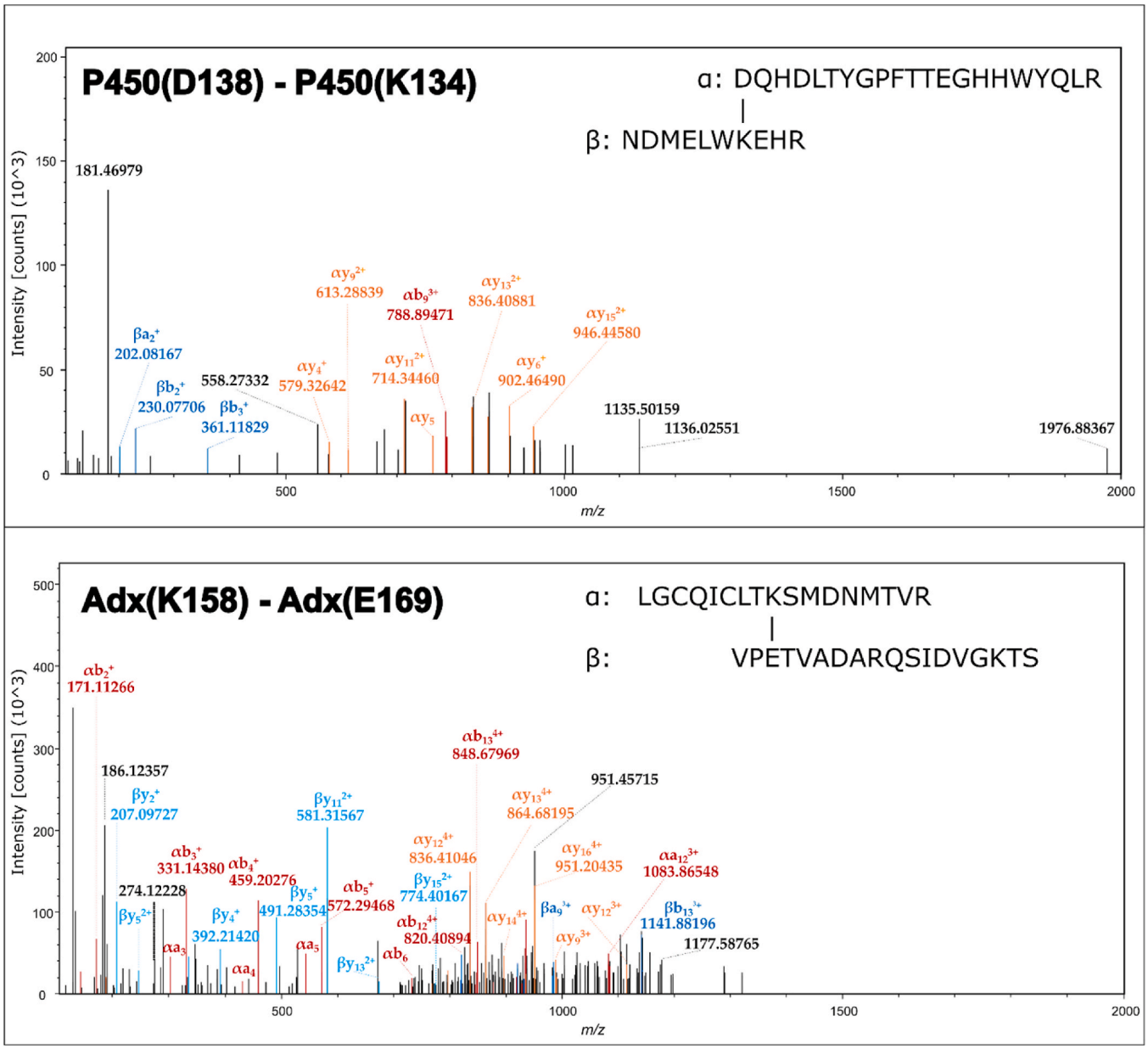

Fig. 4. Example MS/MS spectra of two identified intraprotein crosslinks. The residues crosslinked and the protein of origin are shown in the top left of each spectrum. The isolated peptides containing the crosslinked residues are shown in the top right of each spectrum. The top spectrum is of a P450–P450 intraprotein crosslink identified in sample A1. The bottom spectrum is of an adrenodoxin-adrenodoxin intraprotein crosslink identified in sample A3. Peak colors correspond to identity assigned to peak: black – unassigned, red – a/b type ions assigned to peptide α, orange – y type ions assigned to peptide α, dark blue – a/b type ions assigned to peptide β, and light blue – y type ions assigned to peptide β. (For interpretation of the references to color in this figure legend, the reader is referred to the Web version of this article.)

β-sheet 3 (E504-K496) structures of the AlphaFold prediction of the P450 27A1 complex. The crosslink identified when both adrenodoxin and vitamin D_3 are present (D434-K420) is hard to map to the AlphaFold prediction of P450 27A1 due to disorder in the structure but likely involves a flexible region between β-sheets 1 & 2 as well as a region between β-sheet 1 and α-helix L. This reduction in identified crosslinks when P450 27A1 is in complex with either adrenodoxin or vitamin D_3 is similar to the pattern seen with the interprotein crosslinks described above. Again, this points to the formation of a protein-protein or protein-substrate complex reducing the number of conformations accessed by the P450.

Intraprotein EDC crosslinks of adrenodoxin were also examined in various conditions (Table 4). The bottom spectrum of Fig. 4 shows an example of an adrenodoxin-adrenodoxin intraprotein crosslink. Fig. 5B shows the location of the residues identified from adrenodoxin intraprotein crosslinking analysis modeled on the PDB ID: 3P1M experimental data set. Three crosslinks were identified with isolated adrenodoxin; one of the crosslinks appears twice with different trypsin cleavage products attached. Two of the crosslinks involve the same acidic residue (E169). Two of the crosslinks involve the same basic residues (K158). Therefore, a limited set of four residues (K158, E169, D179, and K182) are implicated in adrenodoxin intraprotein crosslinks. Looking at the positions in the X-ray diffraction crystal structure of human adrenodoxin (PDB ID: 3P1M) [39], D179 and K182 are both located in a flexible region of the structure near the C-terminus. E169 is located right before α-helix E, the last secondary structure resolved before the C-terminal unstructured region. K158 is located in α-helix D. The distance between E169 and K182 is 38.2 Å in the crystal structure

Table 3
P450 27A1 intraprotein crosslinks identified with and without adrenodoxin (Adx) and vitamin D_3 present.

P450 Linked Acidic Site[a]	P450 Linked Basic Site[a]	Isolated P450 27A1 Samples Containing the Crosslink (Out of 3)[c]	P450 27A1 + Vitamin D_3 Samples Containing the Crosslink (Out of 3)[c]	P450 27A1 + Adx Samples Containing the Crosslink (Out of 3)[c]	P450 27A1 + Adx + Vitamin D_3 Samples Containing the Crosslink (Out of 3)[c]
D129	K123	1	1	1	1
D138	K134	1			
E294	K283	1			
D434	K420	1			1
E504	K496[b]	2	2	3	3
E504	K496[b]	1			

[a] Numbering for human P450 27A1 based on Uniprot Accession Q02318.
[b] The peptide identified with the crosslinked basic residue was different between these crosslinked samples. The same crosslink is represented but with different trypsin cleavage products. In the first case, the peptide containing the basic residue is LIQKYK. In the second case, the peptide containing the basic residue is IAELEMQLLLARLIQKYK.
[c] Three crosslinking samples were prepared in parallel from the same protein stocks at the same time and kept separate during workup and analysis.

data. This is too far apart for EDC to crosslink the residues together in an intraprotein crosslink. Two alternative interpretations are possible. First, that this is really an interprotein crosslink from an adrenodoxin dimer that was not fully separated by the SDS-PAGE purification. Second, the adrenodoxin structure is much more flexible than what is suggested by the crystallography data. Regardless of interpretation, the E169-K182 crosslink is not observed when P450 27A1 is also present or when vitamin D_3 is present. It is unclear why the presence of vitamin D_3 would alter adrenodoxin structure. The effect may be related to the 0.49 % (v/v) of ethanol present when substrate is present or may be experimental error. The small amount of ethanol present with substrate was not considered to be significant and was not compensated for in samples without substrate. No adrenodoxin intraprotein crosslinks are observed when P450 27A1 is present. Again, the decrease in observed crosslinks upon complex formation supports that complex formation reduces conformational heterogeneity.

3.3. Molecular modeling

The crosslinking data presented above provide an incomplete picture of how P450 27A1 and adrenodoxin interact. The crosslinking data are most valuable to yield some restraints as to how close some parts of the two proteins must be to one another when interacting. Molecular modeling is required to further interpret this data. A series of molecular modeling steps was performed using the DisVis and HADDOCK software. First, each cluster of interprotein crosslinks was used as restraints with DisVis to determine if the clusters were self-consistent, meaning that all restraints could be simultaneously fulfilled in some orientation of the two-protein complex. All restraints could not be fulfilled at one time. Cluster 1 and cluster 2 restraints could not all be simultaneously fulfilled. Cluster 2 has redundant restraints that may make it impossible to simultaneously fulfill all constraints (multiple crosslinks involve P450 27A1 residue K39). We refined this list to include the cluster 1 and a subset of the presumed closest restraints on the P450 structure based on the AlphaFold structure. The subset of cluster 2 restraints that could work with cluster 1 restraint (P450 K391 – Adx D128) were the P450 K409 – Adx D173, P450 E412 – Adx K182, and P450 D414 – K182 restraints. This subset would be indicative of an adrenodoxin binding site on the proximal side of the P450 enzyme and is consistent with the orientation described by the P450 11A1-Adx and P450 11B2-Adx fusion X-ray crystallography data. Cluster 2 and cluster 3 could not be simultaneously fulfilled, nor could a meaningful subset of these groupings.

Table 4
Adrenodoxin (Adx) intraprotein crosslinks identified with and without P450 27A1 and vitamin D_3 present.

Adx Linked Acidic Site[a]	Adx Linked Basic Site[a]	Isolated Adx Samples Containing the Crosslink (Out of 3)[c]	Adx + Vitamin D_3 Samples Containing the Crosslink (Out of 3)[c]	Adx + P450 27A1 Samples Containing the Crosslink (Out of 3)[c]	Adx + P450 27A1 Vitamin D_3 Samples Containing the Crosslink (Out of 3)[c]
E169	K158	2	1		
E169	K182	2			
D179[b]	K158	1			
D179[b]	K158	1	1		

[a] Numbering for human adrenodoxin based on Uniprot Accession P10109.
[b] The peptide identified with the crosslinked basic residue was different between these crosslinked samples. The same crosslink is represented but with different trypsin cleavage products. In the first case, the C-terminus was a lysine due to cleavage from trypsin (sequence: QSIDVGK). In the second case, the C-terminus was the C-terminus of the entire Adx protein (sequence: QSIDVGKTS).
[c] Three crosslinking samples were prepared in parallel from the same protein stocks at the same time and kept separate during workup and analysis.

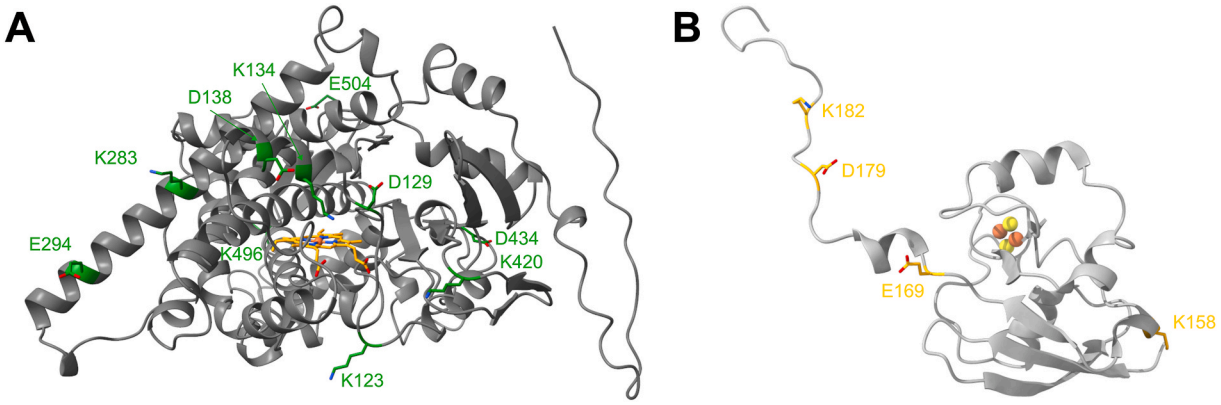

Fig. 5. A. AlphaFold-generated structure of recombinant human P450 27A1. Highlighted as stick drawings in green are residues identified from intraprotein crosslinking analysis. In orange is the approximate position of the heme group as expected from comparison to PDB entry 3N9Y of a P450 11A1-adrenodoxin fusion construct. B. Adrenodoxin structure (PDB: 3P1M). Residues identified in intraprotein crosslinking analysis are shown in gold as stick drawings. The 2Fe–2S cluster of adrenodoxin is shown as yellow and orange spheres. (For interpretation of the references to color in this figure legend, the reader is referred to the Web version of this article.)

This is likely because cluster 2 and cluster 3 are on opposite sides of the P450 structure. Cluster 1 and cluster 3 restraints could be simultaneously fulfilled; however, this leads to a complex structure where the cluster 1 (P450 K391 – Adx D128) restraint is nonsensical. The distance restraint is met but the residue proximity is through the P450 protein surface, which would prevent a crosslink from occurring in real physical space. Therefore, the cluster 1 and cluster 3 grouping was rejected. Cluster 3 by itself can have all restraints fulfilled simultaneously and describes adrenodoxin binding on an allosteric, distal site on the P450. Investigating cluster 1 or 2 restraints by themselves was rejected because remixing those restraints to form a 4-restraint set to describe a proximal binding interface was the best way to allow crosslinking data to inform molecular modeling.

The presence of vitamin D_3 substrate and the persistence of a crosslink do not appear to correlate with the crosslink groupings used to define the proximal and distal binding interfaces. Of the four crosslinks used to define the proximal binding interface, only two remain in crosslinking data with vitamin D_3 present (P450-Adx: K409-D173 and D414-K182). Of the five crosslinks used to define the distal binding interface, only two remain in crosslinking data with vitamin D_3 present (P450-Adx: K509-D128 and K521-D75). Therefore, the modeled protein complexes are likely not capturing the full effects of substrate binding on protein structure dynamics.

After the proximal binding interface and the distal binding interface were defined from preliminary DisVis simulations, more thorough DisVis simulations were performed. This second simulation was used to determine the list of surface-accessible residues likely involved in a P450 27A1 – adrenodoxin complex consistent with the provided crosslinking-based distance restraints. Finally, the HADDOCK software was used to model what possible binding interaction geometries are consistent with the crosslinking restraints. The HADDOCK software uses a scoring function that is a linear combination of various calculated energies for different proposed structures. As pointed out by Glass and colleagues [17], the HADDOCK score gives a larger weighting to van der Waals intermolecular energy than electrostatic interaction energy and distance restraints energy. For P450 enzymes interacting with ferredoxins, the electrostatic interaction is believed to be of primary importance [51]. Also, the distance restraints used here are empirically derived from the

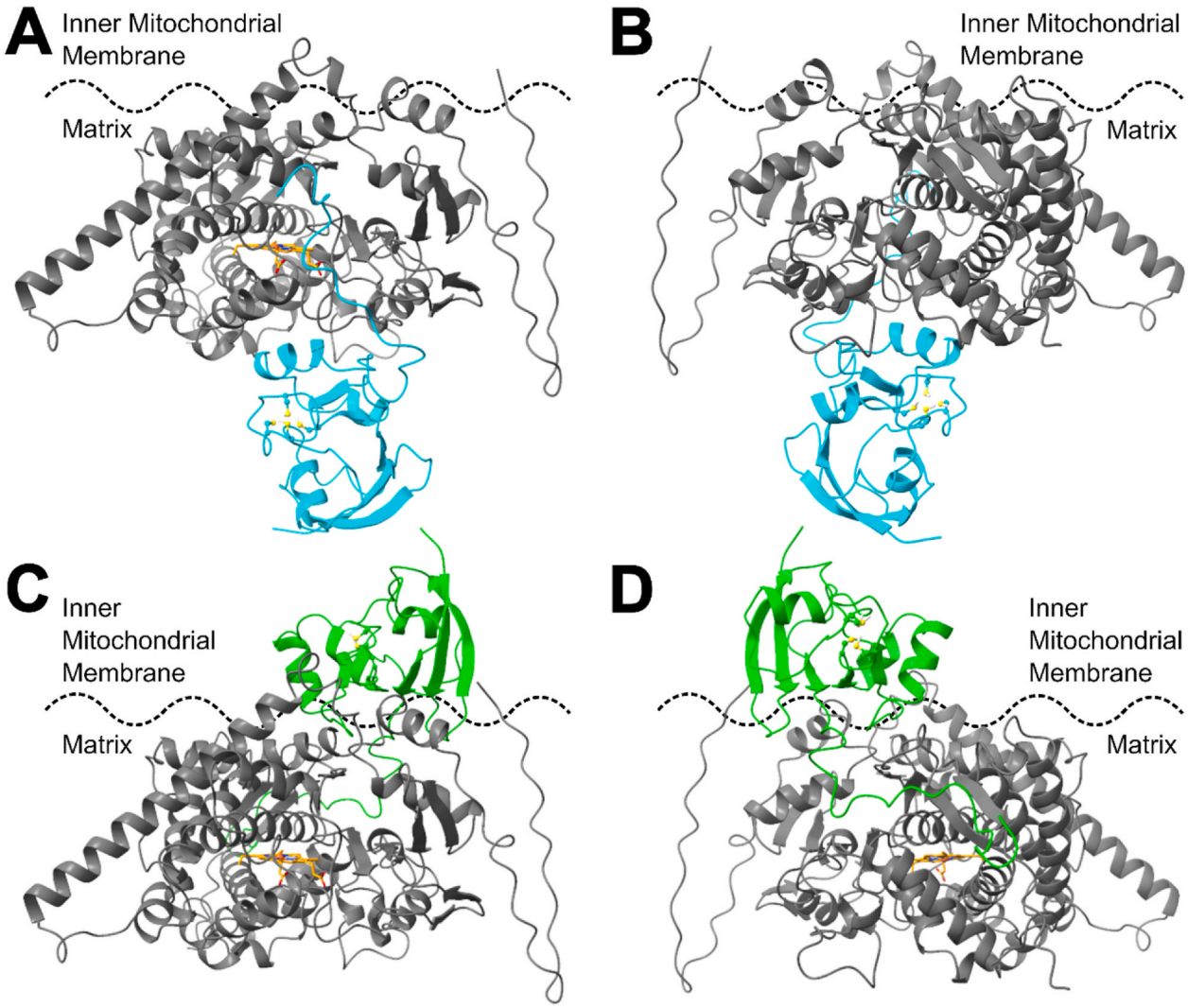

Fig. 6. Representative images of best HADDOCK result complexes for the proximal (A and B) and distal (C and D) binding sites. Subpanels B and D are 180° rotations of subpanels A and C. The P450 27A1 structure is shown in dark grey. The adrenodoxin structure is shown in cyan for the proximal binding site and green for the distal binding site. In orange is the approximate position of the heme group as expected from comparison to PDB entry 3N9Y of a P450 11A1-adrenodoxin fusion construct. The 2Fe–2S cluster of the adrenodoxin can be approximated by the position of the cysteine residues that coordinate the cluster. These are shown as yellow ball and stick structures. The approximate position of the inner mitochondrial membrane is indicated by a dashed black wavy line. The orientation of the protein with respect to the mitochondrial matrix is labeled. (For interpretation of the references to color in this figure legend, the reader is referred to the Web version of this article.)

crosslinking data. It would make sense to weight these energies more significantly. In the cases of the proposed proximal and distal binding interactions simulations performed here, the best overall ranked HADDOCK complexes were also the best ranked complexes based on electrostatic interactions energy and distance restraint energy (weighted by their standard HADDOCK weightings). Because of this consistency in the top-ranked structures, no changes in the HADDOCK score weightings were made. The best HADDOCK overall ranked complexes are further examined.

The proximal (Fig. 6A and B) and distal binding site (Fig. 6C and D) modeling results describe two very different binding sites for adrenodoxin on P450 27A1. They are on different sides of the P450 structure. In the case of the proximal binding site, the orientation is similar to what is seen in the fusion construct experimental structures for P450s 11A1 and 11B2. In these three cases the adrenodoxin is on the proximal side of the P450 heme with α helix 3 of adrenodoxin oriented toward the P450 and the four cysteines (C106, C112, C115, and C152, Uniprot P10109 numbering) that coordinate the 2Fe–2S cluster of adrenodoxin close to the P450 surface near the P450 heme. In the case of the distal binding site, both α helix 2 and 3 of adrenodoxin are oriented toward the P450 indicating a different interaction geometry than the other binding site. Furthermore, the distal binding site geometry would point the four cysteines that coordinate the 2Fe–2S cluster of adrenodoxin away from the P450. Conserved between the two modeling results is that the unstructured C-terminal tail of the adrenodoxin is wrapping around the P450 surface, which could aid in complex stabilization. The modeling results, as an extension of the crosslinking results, support the idea of multiple binding sites available to adrenodoxin on P450 27A1. The proximal binding site described here is most likely similar to the catalytically active position of adrenodoxin based on the orientation and proximity of the adrenodoxin 2Fe–2S cluster with respect to the P450 heme.

3.4. Steady state kinetics

P450 27A1 steady-state reaction parameters were measured at increasing adrenodoxin concentrations to determine the reaction-modulating effects of adrenodoxin. P450 27A1:Adx ratios were 1:1, 1:3, 1:10, and 1:50 with P450 concentration staying constant. As Adx concentrations increased, k_{cat} increased. The value of k_{cat}/K_m decreases with increased adrenodoxin concentration, which led to increased values of K_m (Table 5). The Michaelis-Menten hyperbolic curves of the experiments are shown in Fig. 7. For each condition, three replicates of the reaction were performed. Vitamin D_3 concentrations ranged from 1 to 50 μM for 10-fold and 50-fold Adx but ranged from 1 to 30 μM for 1-fold and 3-fold Adx. Concentrations of vitamin D_3 substrate higher than 50 μM were attempted, but the results were inconsistent likely due to solubility issues. The reported solubility of vitamin D_3 in pure water at 298.2 K is 57 μM [52]. The increased temperature in these experiments should increase solubility, but the buffer conditions would likely decrease solubility. The exact solubility under these conditions is unknown; however, it is likely still near 50 μM. The difference in substrate range between experiments with variable adrenodoxin concentrations is because in the 1-fold and 3-fold Adx experiments substrate saturation was achieved at lower concentrations, as judged by the highest substrate concentration being greater than 4-times the measured K_m. Kinetics data is also deposited as STRENDA ID LNJNJW [53].

3.5. Equilibrium substrate binding titrations

In this study, it was observed that the binding of vitamin D_3 does not elicit a shift in the P450 Soret absorbance, as is often used for tracking ligand binding to P450 enzymes. An alternative method to determine the effects of adrenodoxin on the binding affinity of vitamin D_3 is a competition experiment. In this experiment, the binding affinity of dexmedetomidine hydrochloride (DMM) for P450 27A1 was determined with and without vitamin D_3. When DMM binds to P450 27A1, a noticeable shift in the heme Soret absorbance can be observed, which can be used to generate a difference spectrum [49]. A quadratic fit (Eq. (3)) was used on the binding isotherm obtained from the difference between the absorbance maximum and minimum (typically 434 nm and 413 nm, respectively) plotted against DMM concentrations to determine the apparent K_d of DMM ($K_{dDMMapp}$) if vitamin D_3 was in solution or the real K_d of DMM (K_{dDMM}) if vitamin D_3 was not in solution. Using Eq. (2), K_d of vitamin D_3 (K_{dVD3}) was measured using $K_{dDMMapp}$ and K_{dDMM}, at increasing adrenodoxin concentrations. At all adrenodoxin concentrations, a type II spectral shift was observed for both types of DMM titration. Example binding isotherms and difference spectra for both types of DMM titrations are shown in Fig. 8. For each adrenodoxin concentration, the titration was performed in triplicate. The arrows indicate an increase in peak size as the titrant concentration increased.

Table 6 gives K_{dDMM}, $K_{dDMMapp}$, and K_{dVD3} values measured at increasing adrenodoxin concentrations. The measured K_{dDMM} value with 0 μM adrenodoxin is significantly different ($P < 0.05$) from all the values obtained with adrenodoxin present; however, the values with adrenodoxin present were found to not be statistically different from one another. Using Eq. (2), K_{dVD3} were calculated and found to be within the 95 % confidence interval of each other across different adrenodoxin concentrations and increasing and decreasing unpredictably at increasing adrenodoxin concentrations. One-way ANOVA confirmed that the differences between K_{dVD3} values are statistically insignificant ($\alpha = 0.01$, p values for the comparisons range from 0.2526 to 0.9979).

4. Discussion

The purpose of this study was to investigate the interaction of human cytochrome P450 27A1 and its redox partner protein adrenodoxin to determine structurally how the two proteins interact and whether there is evidence that P450 27A1 catalysis is affected by adrenodoxin other than by electron transfer. Additionally, an aim of this investigation is to compare these results to similar studies with other human mitochondrial P450 enzymes to look for patterns (see review of relevant studies outlined in the introduction section). Fig. S2 in the Supporting Information shows a sequence alignment of human mitochondrial P450 enzymes in which residues identified in various references as important to the P450 and adrenodoxin interaction are highlighted. Outside of mutational studies, no structural method of characterizing the P450 27A1 and adrenodoxin interaction has been reported. Since the EDC crosslinking method has been applied to four out of the seven human mitochondrial P450 enzymes (either directly or indirectly by comparison with a mammalian isoform), it seemed appropriate to continue applying the same method toward completing the set.

Table 5
Kinetic parameters measured from vitamin D_3 hydroxylation by P450 27A1 at increasing concentrations of adrenodoxin (Adx).

[P450]:[Adx] Ratio	k_{cat}, min^{-1} (95 % CI)	K_m, μM (95 % CI)	k_{cat}/K_m, min^{-1} μM^{-1} (95 % CI)
1:1 (1-fold [Adx])	0.0705 (0.0639–0.0770)	0.361 (0.0917–0.630)	0.195 (0.0605–0.330)
1:3 (3-fold [Adx])	0.192 (0.167–0.217)	6.88 (4.68–9.07)	0.0279 (0.0221–0.0337)
1:10 (10-fold [Adx])	0.662 (0.593–0.731)	13.6 (10.2–17.0)	0.0488 (0.0411–0.0565)
1:50 (50-fold [Adx])	1.06 (0.894–1.22)	14.6 (9.19–20.0)	0.0725 (0.0557–0.0893)

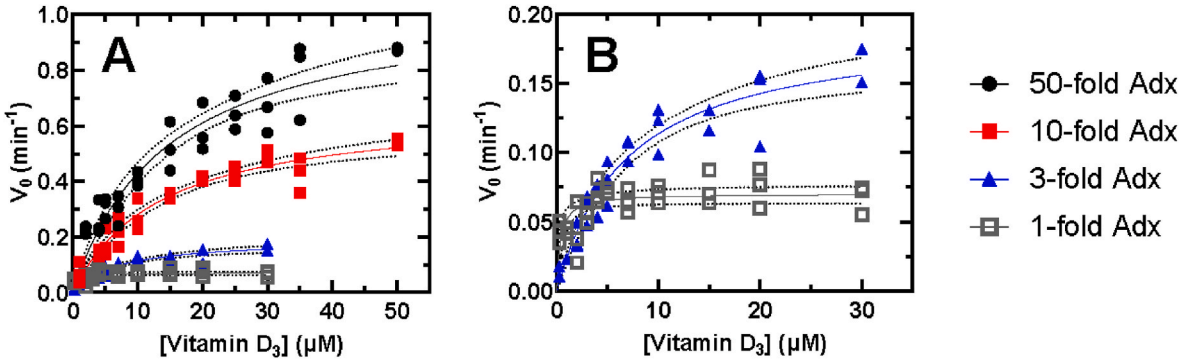

Fig. 7. Steady-state Michaelis-Menten hyperbolic curves of the vitamin D_3 hydroxylation by P450 27A1. A change in rate was observed between 1-fold Adx (grey), 3-fold Adx (blue), 10-fold Adx (red), and 50-fold Adx (black). Experiments were performed in triplicate. Panel A shows all traces. Panel B is a subset of Panel A focused on the 1-fold and 3-fold Adx experiments. The solid lines are the lines of best fit to Eq. (1), and the dotted lines around them are the 95 % confidence bands of each fit. (For interpretation of the references to color in this figure legend, the reader is referred to the Web version of this article.)

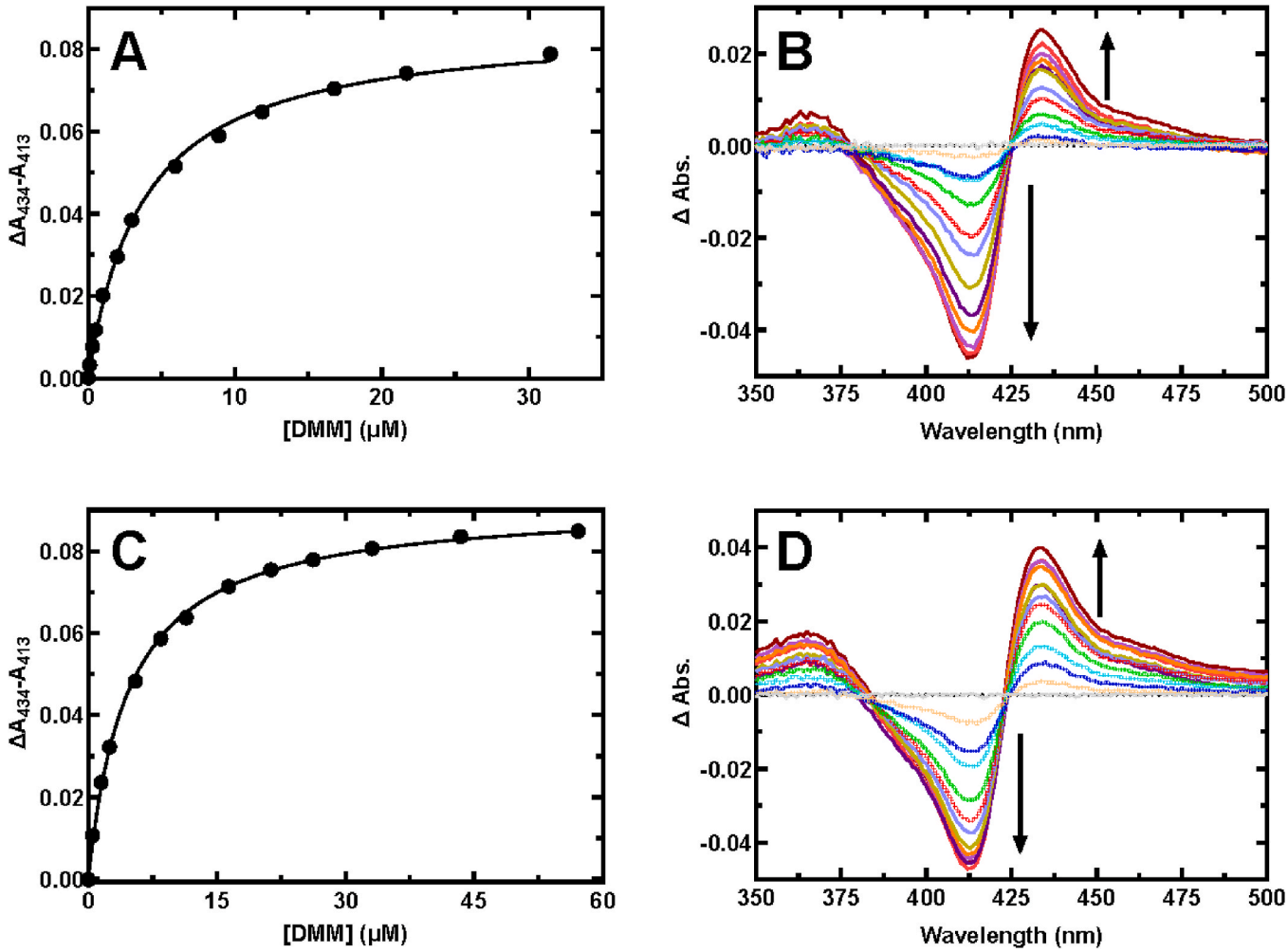

Fig. 8. Binding isotherms and difference spectra of substrate binding to P450 27A1. *A* and *B*, example binding isotherm and difference spectrum, respectively, from DMM binding to P450 27A1 at 10 μM Adx, without vitamin D_3. *C* and *D*, example binding isotherm and difference spectrum, respectively, from DMM binding to P450 27A1 at 10 μM Adx, with 1 μM vitamin D_3.

The results presented in Table 2 for P450 27A1 and adrenodoxin crosslinking by EDC show a larger set of crosslinks identified than in the other reports of EDC crosslinking. The results presented here report 13 distinct crosslinking interactions whereas results for P450 11B1 report 2 [25], for P450 11B2 report 3 [25], for P450 24A1 report 2 [26], and for P450 27C1 report 11 [17]. This difference may primarily be due to starting from a solution phase sample in this work as opposed to an SDS-PAGE resolved sample in the other works. Working from a solution phase sample increases the amount of protein available for protease digestion versus the same amount of protein embedded in gel, which may increase detection of crosslinks. However, it is worth noting that the work with P450 27C1, the P450 with the highest identity to P450 27A1

Table 6
Measured or calculated equilibrium dissociation constants of P450 27A1 with dexmedetomidine (DMM) or vitamin D_3 at increasing concentrations of adrenodoxin (Adx).

[P450]:[Adx] Ratio	K_d DMM (K_{dDMM}) without Vitamin D_3, μM (95 % CI)	K_d DMM ($K_{dDMMapp}$) with 1 μM Vitamin D_3, μM (95 % CI)	K_d Vitamin D_3 (K_{dVD3}), μM (95 % CI)
1:0	5.1 (4.5–5.8)	7.4 (6.5–8.3)	2.3 (1.8–2.7)
1:1 (1-fold [Adx])	3.5 (3.3–3.8)	5.6 (4.7–6.4)	1.8 (1.5–2.0)
1:3 (3-fold [Adx])	3.1 (3.0–3.2)	4.4 (3.9–4.9)	2.4 (2.1–2.7)
1:10 (10-fold [Adx])	2.8 (2.5–3.1)	4.4 (4.0–4.9)	1.7 (1.5–2.0)
1:50 (50-fold [Adx])	3.2 (2.7–3.8)	6.0 (5.4–6.7)	1.2 (0.93–1.4)

(36.80 % based on full Uniport sequence), also has a significantly higher number of identified crosslinks. This raised the question of whether these P450 enzymes bind adrenodoxin in a different manner or tighter to promote more crosslink formation. In one previous study using titrations analyzed by heme Soret band absorbance shift, P450 27A1 was shown to have a stronger interaction (lower K_d) with adrenodoxin than P450 11A1. This was attributed to the presence of arginine 451 in P450 27A1 that is not present in P450 11A1 [23]. While P450 27C1 alone among the other mitochondrial P450s also has an arginine at a similar position, this residue would not be identified by crosslinking studies since EDC does not react with arginine [17]. It would be interesting to perform the relevant arginine to lysine mutation (as done in some cases with the P450 11B subfamily [25]) to see if the residue is then captured in crosslinks. This approach could help determine the role of arginine residues in P450-Adx binding. On the other hand, another study looking at P450-Adx interactions using microscale thermophoresis showed P450 11B2 to have similar if not stronger interactions with adrenodoxin compared to P450s 27A1 and 27C1 [33], and yet another study using surface plasmon resonance reports P450 11A1 has a stronger interaction with adrenodoxin than P450s 11B1 and 11B2 [54]. No other study has used the same method to evaluate the P450-Adx K_d binding constants, so it is difficult to correlate the adrenodoxin binding strength to crosslink number. Moreover, crosslink number can be impacted by factors other than binding strength like peptide ionization and protein sequence coverage. Regardless of the effect on thermodynamic binding strength, the presence of this additional arginine may encourage greater interaction time between a P450 and adrenodoxin, leading to a greater chance of crosslink development regardless of actual residues involved.

Another important comparison to make across the various P450-Adx crosslinking studies is the actual residues identified. A lysine at the same relative position as residue K391 in P450 27A1 is conserved in all seven human mitochondrial P450 enzymes and is the only lysine conserved across all seven P450 enzymes. Lysine 391 is the only P450 27A1 residue observed in our crosslinking data that also appears in the crosslinking results of other P450 enzymes. (Residue numbering for other P450 enzymes is based on Uniprot entries: P450 11A1 - P05108, P450 11B1 – P15538, P450 11B2 – P19099, P450 24A1 - Q07973, P450 27A1 - Q02318, P450 27B1 – O15528, and P450 27C1 - Q4G0S4.) The corresponding lysine in P450s 11B1 (K370), 11B2 (K370), and 24A1 (K382) was observed in crosslinking studies but not in the crosslinking study in P450 27C1 [17,25,26]. Lysine 391 is also of note because it is the only residue of three (K387, K391, and R451) identified by Pikuleva and colleagues as important to the P450 27A1 and adrenodoxin interaction, based on mutational studies of P450 27A1 activity and/or studies of P450 27A1 and adrenodoxin binding affinity, that is also found in our crosslinking data [23]. The corresponding lysine in P450 11A1 (K378) has also been identified as important based on mutational studies [20,22]. The corresponding lysine in P450 11B2 (K370) was identified by inspection of the P450 11B2 – adrenodoxin fusion construct as important to the complex interaction [14]. Finally, modeled structures of P450 27B1 and adrenodoxin suggest that the corresponding lysine (K375) in P450 27B1 is also important to complex formation [24]. The consistency of this lysine appearing in crosslinking studies, fusion construct structural studies, and mutational studies implies that its conservation across all of the human mitochondrial P450 enzymes may be a key point for the P450 and adrenodoxin interaction.

There are two omissions from our P450 27A1 crosslinking data worth highlighting. The P450 11B1 and 11B2 crosslinking data identified K357 in crosslinks to adrenodoxin but the corresponding K378 in P450 27A1 was not observed [25]. The P450 27C1 crosslinking data identified K181 in crosslinks to adrenodoxin but the corresponding K167 in P450 27A1 was not observed [17]. These differences in P450 crosslinking residues suggest that while some conservation of the interaction exists, there is also flexibility in how this interaction can develop between different P450 enzymes.

There is also variability in the residues involved in crosslinks from adrenodoxin across the different crosslinking studies: D132 of adrenodoxin shows up in crosslinks with P450s 27C1 and 27A1, D139 shows up in crosslinks with P450s 11B1, 11B2, and 27C1, E169 shows up in crosslinks with P450s 24A1 and 27A1, and D173 shows up in crosslinks with P450s 11B1, 11B2, and 27A1. However, the residues on the P450 that these conserved adrenodoxin residues are crosslinked to varies. For example, the P450 27A1 K391 crosslink that is conserved in the corresponding lysine in P450s 11B1, 11B2 and 24A1 are all linked to different adrenodoxin residues: Adx D139 with P450 11B1, Adx D136 with P450 11B2, Adx E95 with P450 24A1, and Adx D128 with P450 27A1 [17,25,26]. One conserved pattern is that many of the adrenodoxin crosslinked residues are in α helix 3 of adrenodoxin which has been highlighted as key for the P450 and adrenodoxin interaction by both NMR and fusion construct structural studies [14,27,55]. Additionally of note is that K182 of adrenodoxin appears in crosslinks with both P450 27A1 and 27C1. This is counter to the conventional view that adrenodoxin contributes acidic residues and P450 enzymes contributes basic residues. In total, the variation in adrenodoxin participation in the different crosslinking studies further emphasizes that the interaction is flexible and variable between P450 enzymes even though they use the same redox partner.

Another way in which these crosslinking results with P450 27A1 vary from other studies is the apparent effect of adrenodoxin and/or substrate on P450 structure. The results in Tables 2 and 3 show a decrease in the number of interprotein and intraprotein crosslinks identified when either adrenodoxin or vitamin D_3 is added to solution with P450 27A1. There does not appear to be any further reductive effect of having both adrenodoxin and vitamin D_3 present. Our interpretation of this finding is that the presence of either redox partner or substrate affects the accessible conformational space of the P450 enzyme. In their crosslinking study with P450 24A1, Kumar and colleagues reach a similar conclusion but from a different approach [26]. In their discussion of conformational effects, they focus on P450 intraprotein crosslinks. They find additional P450 intraprotein crosslinks in their data when adrenodoxin is in solution, and they suggest that a new P450 conformation is induced when adrenodoxin is bound. Furthermore, they find that while substrate alone does not induce changes in P450 intraprotein crosslinking, the presence of both substrate and redox partner further promotes structural changes in the P450 compared to adrenodoxin alone. Therefore, presence of substrate and redox partner have a synergistic effect on P450 structure with P450 24A1 but not P450 27A1, and the presence of redox partner increases conformational variability with P450 24A1 but decreases it with P450 27A1. This conclusion needs to be examined with techniques that better examine the entire protein structure to confirm this pattern is not due to

limitations of the crosslinking method to surface residues and only aspartates, glutamates, and lysines.

The crosslinking results in this study are intended to provide rough guidelines for modeling protein-protein interactions and are not intended to be viewed as fully accurate representations of all interacting residues of the proteins. This is due to the limited reactivity of EDC as noted earlier. Also, this is due to the non-physiological conditions of the crosslinking reactions. The reactions were performed without lipid membranes or membrane mimics. The presence and identity of lipids is known to affect P450 27A1 activity; therefore, the presence of lipids will almost certainly affect protein conformational equilibrium and the accessibility of different parts of the protein. Furthermore, the proteins used were all produced in *E. coli* and would not have post-translational modifications present in native cell production. This is relevant because both the P450 27A1 UniProt record (Q02318) and another study indicate modification of lysine residues by acetylation or arachidonate oxidation products [56]. These references highlight lysine residues appearing in the crosslinking results (K391, K509, K520). Other post-translational modifications (e.g., glycosylation, phosphorylation) would also likely alter the interaction between the proteins. Finally, we may expect different crosslinking results with different substrates as others have noted the P450-adrenodoxin interaction changes with P450 11A1 depending on whether cholesterol or vitamin D_3 is present [57]. Regardless of these limitations, the crosslinking data still informs our understanding of the preferences for protein interaction.

By using the crosslinking interactions as restraints, two different adrenodoxin binding sites on P450 27A1 were generated from modeling work. The distal site is unlike anything reported for human mitochondrial P450 interactions previously; however, Glass and coworkers report alternative bindings sites for adrenodoxin on P450 27C1, including allosteric sites [17]. The result presented in our study possibly represents either a poorly populated allosteric site or an over analysis of spurious crosslink noise. The distal binding site is most likely not physiologically relevant as it would require adrenodoxin to be present in the inner mitochondrial membrane or a significant reorientation of the P450 enzyme (see Fig. 6C and D). Furthermore, the change in distance and orientation from the [2Fe–2S] cluster to the heme would significantly alter electron transfer rates. If two adrenodoxin binding sites are bound at the same time, one might expect to see an 80–85 kDa band in lane 7 of the SDS-PAGE result of Fig. 1. There are faint bands in this molecular weight range in Fig. 1; however, more detailed structural data would be needed to conclude the possibility of complexes other than the 1:1 stoichiometry.

The proximal binding site result shown in Fig. 6A and B is proposed to be similar to an active complex structure and can be compared to other proposed complex structures. Using the Matchmaker tool in ChimeraX, the predicted structure of the P450 27A1-adrenodoxin complex was aligned with the P450 11A1 (Fig. S3) and P450 11B2 – adrenodoxin fusion constructs. There is good alignment between the P450 complexes. The RMSD of the P450 11A1 domain of the experimental structure to the P450 27A1 domain of the predicted structure is 1.158 Å between 350 pruned atoms pairs and 2.712 Å across all 463 pairs, this excludes the adrenodoxin domain. The RMSD of the P450 11B2 domain of the experimental structure to the P450 27A1 domain of the predicted structure is 1.220 Å between 311 pruned atom pairs and 3.547 Å across all 459 pairs, this excludes the adrenodoxin domains. “Pruned atom pairs” refers to the subset of all atom pairings where ChimeraX has removed atom pairings structurally distant from one another. The P450 domains are fairly well-aligned; however, the adrenodoxin domains are more variable. The experimental adrenodoxin structural data do not resolve all the adrenodoxin residues, so RMSD calculations cannot be done for the entire structure. The RMSD of the peptide backbone of the 67 residues present in all three adrenodoxin structures is 9.771 Å between the adrenodoxin domain of the P450 11A1 fusion and adrenodoxin domain of the proximal binding site result and is 10.660 Å between the P450 11B2 fusion adrenodoxin domain and the adrenodoxin domain of the proximal binding site result. For reference, the adrenodoxin domains of the two fusion constructs have a much smaller RMSD of 1.998 Å. Upon visual inspection, the adrenodoxin domain of the proximal binding site modeling result from this work appears rotated from orientation of the fusion constructs (see Fig. S3 in the Supporting Information). This rotation forces the 2Fe–2S cluster site of the adrenodoxin further away from the heme iron atom (~25 Å) compared to the distance in the fusion proteins (~20 Å). The ~25 Å distance in our result with P450 27A1 is similar to the 26.1 Å result reported for crosslink-restraint driven computational docking of P450 27C1 with adrenodoxin [17]. Despite these differences in orientation and redox center distances, the adrenodoxin in our modeling result does mostly have the same secondary structures and tertiary fold as the fusion experimental structures except that small α helices 4 and 5 present in the experimental data are missing from our modeling result. Additionally, α helix 3 of adrenodoxin, previously suggested by others as most responsive to P450 binding [55], is closest to the heme in the respective P450 structures. In total, it appears that the proximal binding site described by crosslinking restrictions and predicted by modeling yields a similar interaction to the fusion construct data but with a twist on the orientation. The differences between the modeling data and the experimental structural data could be due to limitations in the modeling approach or could be due to limitations in conformational freedom of the interactions of the fusion constructs since the two protein domains in the fusion constructs are bound by a linker of definite length and limited conformational flexibility. Experimental structural data of a non-linked P450 and adrenodoxin dimer complex would aid in determining the appropriate orientation of the adrenodoxin with respect to the P450.

Subsequent to reporting crosslinking data, the effects of varied adrenodoxin concentrations on P450 27A1 reactivity with the substrate vitamin D_3 were studied. These results are shown in Fig. 7 and Table 5. The best comparison of our steady state data to other P450 27A1 data is from the work of Sawada and coworkers. In their study, they found the k_{cat} and K_m values of the P450 27A1 and vitamin D_3 reaction to be 0.27 min^{-1} and 3.2 μM, respectively, with protein concentrations of 0.1 μM P450, 2.0 μM adrenodoxin, and 0.2 μM adrenodoxin reductase [58]. Our k_{cat} value is 2.5–3.9-fold faster for the P450:Adx ratios closest to theirs, and our K_m value is 4.3–4.6-fold larger. Therefore, our values are different but within a factor of 5-fold range. The discrepancy in kinetic parameters is likely due to their use of unpurified P450 still in *E. coli* membrane fractions as opposed to our approach of isolated and purified P450 enzyme. Their use of membrane fractions would change the local environment around the P450 compared to our buffered solution environment. Measuring P450 27A1 kinetics in lipid membranes or cyclodextrin changes the observed kinetics [30]. Different phospholipids in solution with P450 27A1 can have variable effects on enzyme kinetics and substrate binding [59]. Variation in enzyme function with different phospholipids has also been observed with other P450 enzymes [60]. This effect varies for different substrates and P450 enzymes and would need to be studied specifically for this reaction to determine its contribution to the observed difference in kinetic parameters.

The overall trends of our experiment with varying adrenodoxin concentrations are that with increasing adrenodoxin concentration the k_{cat} of the reaction increases, the k_{cat}/K_m of the reaction decreases, and consequently the K_m of the reaction increases. If either of the adrenodoxin mediated reduction steps in the P450 catalytic cycle are rate-limiting, it would make sense that the k_{cat} of the reaction increases with increasing adrenodoxin as increasing the population of reduced adrenodoxin in solution should speed up the overall reaction. This is what is observed in this case.

The adrenodoxin reductase mediated reduction of adrenodoxin, which must occur before reduction of the P450, is not rate-limiting and therefore not contributing to the reported adrenodoxin concentration effects on P450 27A1 catalysis. A previous study has determined the kinetic parameters of the adrenodoxin reductase and adrenodoxin reaction [33]. Based on those values, the adrenodoxin reductase and

adrenodoxin reaction under the lowest adrenodoxin concentration studied here is nearly 1000-fold faster than the P450 reaction. The adrenodoxin reductase reaction is proceeding at a velocity (v) of 13 μM/min whereas the P450 27A1 reaction has a v of 0.014 μM/min. The adrenodoxin reductase reaction should also not be limited by reagent concentrations either. Once the adrenodoxin transfers electrons to the P450, it is able to be reduced again by adrenodoxin reductase. Furthermore, the NADPH concentrations are at least initially 100-fold greater than the adrenodoxin concentration. The amount of NADPH needed to support the amount of product produced in the most optimal conditions (50-fold adrenodoxin and 50 μM vitamin D_3) is only approximately 3 μM NADPH, ignoring uncoupling. Therefore, the excess NADPH, recycling of adrenodoxin, and fast adrenodoxin reductase reaction should mean any observed trend in changes to the P450 kinetic parameters is due primarily to that reaction.

Interestingly, the k_{cat}/K_m value for the P450 reaction decreases with increasing adrenodoxin concentration. The parameter k_{cat}/K_m can be considered an efficiency rate constant that reports on the probability that the substrate reacts rather than dissociating, also referred to as catalytic specificity [48]. By this definition, the data presented here suggests that with increasing adrenodoxin concentration, the vitamin D_3 substrate is more likely to dissociate than be converted to product. This is counterintuitive as we have already seen that the overall reaction rate is faster with more adrenodoxin present. That interpretation is supported by the calculated value of K_m decreasing with increasing adrenodoxin concentration. The simple interpretation of this trend is that adrenodoxin presence discourages vitamin D_3 binding; however, this is based on a common misconception that the Michaelis constant K_m is equivalent to the substrate dissociation constant K_d. These two constants are only the same in cases where substrate binding equilibrium is rapid compared to catalytic turnover. K_m is therefore difficult to interpret directly in most cases [48].

We further examined the effect of adrenodoxin concentration on substrate binding via equilibrium titration (Fig. 8 and Table 6) and found adrenodoxin concentration had no effect on the vitamin D_3 equilibrium dissociation constant (K_d). Taken together, these data suggest that for P450 27A1 and vitamin D_3, the presence of excess adrenodoxin causes vitamin D_3 to more often dissociate from the enzyme in a reaction step past initial binding/unbinding but prior to product formation. This could be explained by changes in kinetics of later reaction steps like oxygen binding or P450 reduction and may be observable by directly studying these steps or other general parameters like NADPH reaction coupling and stability of P450-oxy complexes. The nature of the change in P450 enzyme activity could be due to a shift in P450 conformational state either due to direct adrenodoxin interaction or indirect molecular crowding effects. Further detailed kinetic studies of this reaction will be required to parse all effects of adrenodoxin on P450 27A1 catalysis and their origins.

The adrenodoxin effects on steady state kinetics parameters and equilibrium binding constants observed here can be compared to data with other human mitochondrial P450 enzymes. The most complete comparison is to the reactions of human P450s 11B1 and 11B2 with varying adrenodoxin concentrations [13,14]. In both cases, increasing adrenodoxin concentration compared to the P450 concentrations in ratios similar to this study showed that with increasing adrenodoxin concentration the k_{cat} of the reaction increases, the k_{cat}/K_m of the reaction increases, the K_m of the reaction decreases, and the value of substrate K_d decreases (the change in K_d is less dramatic with P450 11B2). Thus, in the case of the human P450 11B enzymes, adrenodoxin does appear to increase reaction efficiency by encouraging substrate binding. No studies on other human mitochondrial P450 enzymes have looked at the effect of multiple adrenodoxin concentrations on both steady state kinetics and substrate equilibrium binding. However, different studies have examined the binding of substrate to human mitochondrial P450 enzymes with at least one adrenodoxin concentration and without adrenodoxin. Studies on P450 11A1 [15], P450 24A1 [16], and P450 27C1 [17] with their respective substrates show no significant change in substrate binding K_d when adrenodoxin is added to solution. With the results from this study on P450 27A1 and only human P450 27B1 missing from the list of human mitochondrial P450 enzymes where substrate binding has been studied with and without adrenodoxin, it appears the effect of adrenodoxin to enhance substrate binding to the P450 11B enzymes is the exception and not the rule.

5. Conclusions

In conclusion, this work examined the interaction of human cytochrome P450 27A1 with adrenodoxin. Chemical crosslinking of the two proteins followed by mass spectrometry crosslink verification adduce that the two proteins primarily form a 1:1 protein complex but may do so in multiple orientations. Two binding sites for adrenodoxin on P450 27A1 were suggested by using the crosslinking data as restraints for molecular modeling of the protein complex. Analysis of the interprotein and intraprotein crosslinks formed under varying conditions with adrenodoxin and/or substrate present revealed that the presence of either adrenodoxin or substrate limits the conformational space accessed by the P450 enzyme. Studies of P450 27A1 steady state kinetics showed that increasing the concentration of adrenodoxin in these studies increases reaction k_{cat}, decreases k_{cat}/K_m, and increases K_m. Follow-up studies of substrate binding equilibrium constant (K_d) with increasing adrenodoxin concentration show no effect of adrenodoxin concentration on binding constant. This implies that the trends observed in the kinetics data are not simply explained by a change in the affinity of substrate for the enzyme in the initial binding step. Further studies of other reaction steps with varied adrenodoxin concentration will need to be performed to determine what causes decreased reaction efficiency (k_{cat}/K_m).

When compared to similar studies of adrenodoxin with other human mitochondrial P450 enzymes, there are different outcomes depending on the P450 enzyme being examined. Studies of P450s 11B1, 11B2, 24A1, and 27C1 do not yield consistent crosslinking results and show limited overlap with the results presented here. P450 24A1 appears to have increased conformational flexibility in the presence of adrenodoxin, whereas P450 27A1 appears to have decreased conformational access. P450s 11B1 and 11B2 have stimulated reaction efficiency (increased k_{cat}/K_m) and increased substrate affinity (decreased K_d) in the presence of adrenodoxin, whereas P450 27A1 has decreased reaction efficiency and no change in substrate affinity. Altogether, these comparisons show while there is some conservation in the human P450-adrenodoxin interaction, significant differences in binding complex formation and functional impact of adrenodoxin varies from P450 to P450. Since the adrenodoxin interaction is key to catalytic activity, it is therefore possible to modulate P450 activity by affecting the P450-adrenodoxin interaction. The differences in the interactions among the P450 enzymes may suggest that it is possible to selectively modulate the activity of one P450 enzyme without affecting the others. This could lead to new approaches to studying mitochondrial P450 enzymes or clinical treatments based on altering the interaction of the P450s with adrenodoxin.

CRediT authorship contribution statement

Quoc T. Vu: Writing – original draft, Validation, Investigation, Formal analysis. **Katherine C. May:** Validation, Investigation, Formal analysis. **Leonard B. Collins:** Writing – review & editing, Validation, Methodology, Investigation, Formal analysis, Data curation, Conceptualization. **Ying Xi:** Validation, Methodology, Investigation, Formal analysis, Data curation. **Zachary B. Davis:** Resources, Investigation. **Jackson L. Bartholomew-Schoch:** Resources. **Lindsay R. Vaughn:** Resources. **Katherine R. Provost:** Resources. **Noah L. Arnold:** Investigation. **Ethan F. Harris:** Investigation. **Emma K. Stone:** Resources. **Hayden K. Campbell:** Investigation. **Lyndsay M. Snider:** Investigation.

Taufika Islam Williams: Writing – review & editing, Supervision, Methodology, Conceptualization. **Michael J. Reddish:** Writing – review & editing, Writing – original draft, Visualization, Validation, Supervision, Project administration, Methodology, Investigation, Funding acquisition, Formal analysis, Conceptualization.

Funding and additional information

This material is based upon work supported by the National Science Foundation under Award No. 2213207 (M J R). Any opinions, findings and conclusions or recommendations expressed in this material are those of the author(s) and do not necessarily reflect the views of the National Science Foundation. This project was also supported by startup funding from the Department of Chemistry and Fermentation Sciences at Appalachian State University. This work was performed in part by the Molecular Education, Technology and Research Innovation Center (METRIC) at NC State University, which is supported by the State of North Carolina.

Declaration of competing interest

The authors declare that they have no conflicts of interest with the contents of this article.

Acknowledgments

Molecular graphics and analyses performed with UCSF ChimeraX, developed by the Resource for Biocomputing, Visualization, and Informatics at the University of California, San Francisco, with support from National Institutes of Health R01-GM129325 and the Office of Cyber Infrastructure and Computational Biology, National Institute of Allergy and Infectious Diseases.

The FP7 WeNMR (project# 261572), H2020 West-Life (project# 675858), the EOSC-hub (project# 777536) and the EGI-ACE (project# 101017567) European e-Infrastructure projects are acknowledged for the use of their web portals, which make use of the EGI infrastructure with the dedicated support of CESNET-MCC, INFN-LNL-2, NCG-INGRID-PT, TW-NCHC, CESGA, IFCA-LCG2, UA-BITP, TR-FC1-ULAKBIM, CSTCLOUD-EGI, IN2P3-CPPM, CIRMMP, SURFsara and NIKHEF, and the additional support of the national GRID Initiatives of Belgium, France, Italy, Germany, the Netherlands, Poland, Portugal, Spain, UK, Taiwan and the US Open Science Grid.

Appendix A. Supplementary data

Supplementary data to this article can be found online at https://doi.org/10.1016/j.abb.2025.110700.

Data availability

Gel images, unprocessed high-performance liquid chromatography traces used for enzyme kinetics, processed kinetics data, unprocessed spectral data for binding studies, and processed spectral binding curve data are available to be shared upon request from the corresponding author (Michael Reddish) at reddishmj@appstate.edu.

Raw MS data and Proteome Discoverer data files are available online on the website PanoramaWeb under the NCSU – METRIC Public Data repository ()https://panoramaweb.org/NCSU%20-%20METRIC/project-begin.view.

Kinetics data experimental description and is also as STRENDA ID LNJNJW and available at https://doi.org/10.22011/strenda_db.LNJNJW.

References

[1] S. Rendic, F.P. Guengerich, Survey of human oxidoreductases and cytochrome P450 enzymes involved in the metabolism of xenobiotic and natural chemicals, Chem. Res. Toxicol. 28 (1) (2015) 38–42.
[2] F.P. Guengerich, Intersection of the roles of cytochrome P450 enzymes with xenobiotic and endogenous substrates: relevance to toxicity and drug interactions, Chem. Res. Toxicol. 30 (1) (2017) 2–12.
[3] F.P. Guengerich, Human cytochrome P450 enzymes, in: P.R. Ortiz de Montellano (Ed.), Cytochrome P450: Structure, Mechanism, and Biochemistry, Springer, New York, 2015, pp. 523–785.
[4] V.M. Kramlinger, L.D. Nagy, R. Fujiwara, K.M. Johnson, T.T.N. Phan, Y. Xiao, J. M. Enright, M.B. Toomey, J.C. Corbo, F.P. Guengerich, Human cytochrome P450 27C1 catalyzes 3,4-desaturation of retinoids, FEBS (Fed. Eur. Biochem. Soc.) Lett. 590 (9) (2016) 1304–1312.
[5] Z. Li, Y. Jiang, F.P. Guengerich, L. Ma, S. Li, W. Zhang, Engineering cytochrome P450 enzyme systems for biomedical and biotechnological applications, J. Biol. Chem. 295 (3) (2020) 833–849.
[6] L. Waskell, J.-J.P. Kim, Electron transfer partners of cytochrome P450, in: P. R. Ortiz de Montellano (Ed.), Cytochrome P450: Structure, Mechanism, and Biochemistry, Springer, New York, 2015, pp. 33–68.
[7] D. Batabyal, L.S. Richards, T.L. Poulos, Effect of redox partner binding on cytochrome P450 conformational dynamics, J. Am. Chem. Soc. 139 (37) (2017) 13193–13199.
[8] S.H. Liou, M. Mahomed, Y.T. Lee, D.B. Goodin, Effector roles of putidaredoxin on cytochrome P450cam conformational states, J. Am. Chem. Soc. 138 (32) (2016) 10163–10172.
[9] S. Tripathi, H. Li, T.L. Poulos, Structural basis for effector control and redox partner recognition in cytochrome P450, Science 340 (6137) (2013) 1227–1230.
[10] S.S. Pochapsky, T.C. Pochapsky, J.W. Wei, A model for effector activity in a highly specific biological electron transfer complex: the cytochrome P450(cam)-putidaredoxin couple, Biochemistry 42 (19) (2003) 5649–5656.
[11] M.C. Glascock, D.P. Ballou, J.H. Dawson, Direct observation of a novel perturbed oxyferrous catalytic intermediate during reduced putidaredoxin-initiated turnover of cytochrome P-450-CAM: probing the effector role of putidaredoxin in catalysis, J. Biol. Chem. 280 (51) (2005) 42134–42141.
[12] J.D. Lipscomb, S.G. Sligar, M.J. Namtvedt, I.C. Gunsalus, Autooxidation and hydroxylation reactions of oxygenated cytochrome P-450cam, J. Biol. Chem. 251 (4) (1976) 1116–1124.
[13] C.L. Loomis, S. Brixius-Anderko, E.E. Scott, Redox partner adrenodoxin alters cytochrome P450 11B1 ligand binding and inhibition, J. Inorg. Biochem. 235 (2022) 111934.
[14] S. Brixius-Anderko, E.E. Scott, Structural and functional insights into aldosterone synthase interaction with its redox partner protein adrenodoxin, J. Biol. Chem. 296 (2021) 100794.
[15] K.D. McCarty, L. Liu, Y. Tateishi, H.L. Wapshott-Stehli, F.P. Guengerich, The multistep oxidation of cholesterol to pregnenolone by human cytochrome P450 11A1 is highly processive, J. Biol. Chem. 300 (1) (2024) 105495.
[16] N. Jay, S.R. Duffy, D.F. Estrada, Characterization of a cleavable fusion of human CYP24A1 with adrenodoxin reveals the variable role of hydrophobics in redox partner binding, Biochemistry 61 (2) (2022) 57–66.
[17] S.M. Glass, S.N. Webb, F.P. Guengerich, Binding of cytochrome P450 27C1, a retinoid desaturase, to its accessory protein adrenodoxin, Arch. Biochem. Biophys. 714 (2021) 109076.
[18] T.B. Adamovich, I.A. Pikuleva, V.L. Chashchin, S.A. Usanov, Selective chemical modification of cytochrome P-450SCC lysine residues. Identification of lysines involved in the interaction with adrenodoxin, Biochim. Biophys. Acta Protein Struct. Mol. Enzymol. 996 (3) (1989) 247–253.
[19] N.V. Strushkevich, T.N. Azeva, G.I. Lepesheva, S.A. Usanov, Role of positively charged residues Lys267, Lys270, and Arg411 of cytochrome P450scc (Cyp11A1) in interaction with adrenodoxin, Biochemistry (Mosc.) 70 (6) (2005) 664–671.
[20] J. Tuls, L. Geren, F. Millett, Fluorescein isothiocyanate specifically modifies lysine 338 of cytochrome P-450scc and inhibits adrenodoxin binding, J. Biol. Chem. 264 (28) (1989) 16421–16425.
[21] S.A. Usanov, S.E. Graham, G.I. Lepesheva, T.N. Azeva, N.V. Strushkevich, A. A. Gilep, R.W. Estabrook, J.A. Peterson, Probing the interaction of bovine cytochrome P450scc (CYP11A1) with adrenodoxin: evaluating site-directed mutations by molecular modeling, Biochemistry 41 (26) (2002) 8310–8320.
[22] A. Wada, M.R. Waterman, Identification by site-directed mutagenesis of two lysine residues in cholesterol side chain cleavage cytochrome P450 that are essential for adrenodoxin binding, J. Biol. Chem. 267 (32) (1992) 22877–22882.
[23] I.A. Pikuleva, C. Cao, M.R. Waterman, An additional electrostatic interaction between adrenodoxin and P450c27 (CYP27A1) results in tighter binding than between adrenodoxin and P450scc (CYP11A1), J. Biol. Chem. 274 (4) (1999) 2045–2052.
[24] N. Urushino, K. Yamamoto, N. Kagawa, S. Ikushiro, M. Kamakura, S. Yamada, S. Kato, K. Inouye, T. Sakaki, Interaction between mitochondrial CYP27B1 and adrenodoxin: role of arginine 458 of mouse CYP27B1, Biochemistry 45 (14) (2006) 4405–4412.
[25] H.M. Peng, R.J. Auchus, Molecular recognition in mitochondrial cytochromes P450 that catalyze the terminal steps of corticosteroid biosynthesis, Biochemistry 56 (17) (2017) 2282–2293.
[26] A. Kumar, P.R. Wilderman, C. Tu, S. Shen, J. Qu, D.F. Estrada, Evidence of allosteric coupling between substrate binding and Adx recognition in the vitamin D carbon-24 hydroxylase CYP24A1, Biochemistry 59 (15) (2020) 1537–1548.

[27] N. Strushkevich, F. MacKenzie, T. Cherkesova, I. Grabovec, S. Usanov, H.W. Park, Structural basis for pregnenolone biosynthesis by the mitochondrial monooxygenase system, Proc. Natl. Acad. Sci. U. S. A. 108 (25) (2011) 10139–10143.
[28] I.H. Betsholtz, K. Wikvall, Cytochrome P450 CYP27-catalyzed oxidation of C27-steroid into C27-acid, J. Steroid Biochem. Mol. Biol. 55 (1) (1995) 115–119.
[29] R.C. Tuckey, W. Li, D. Ma, C.Y.S. Cheng, K.M. Wang, T.K. Kim, S. Jeayeng, A. T. Slominski, CYP27A1 acts on the pre-vitamin D3 photoproduct, lumisterol, producing biologically active hydroxy-metabolites, J. Steroid Biochem. Mol. Biol. 181 (2018) 1–10.
[30] E.W. Tieu, W. Li, J. Chen, D.M. Baldisseri, A.T. Slominski, R.C. Tuckey, Metabolism of cholesterol, vitamin D3 and 20-hydroxyvitamin D3 incorporated into phospholipid vesicles by human CYP27A1, J. Steroid Biochem. Mol. Biol. 129 (3–5) (2012) 163–171.
[31] S. Ayadi, S. Friedrichs, R. Soules, L. Pucheu, D. Lutjohann, S. Silvente-Poirot, M. Poirot, P. de Medina, 27-Hydroxylation of oncosterone by CYP27A1 switches its activity from pro-tumor to anti-tumor, J. Lipid Res. 64 (12) (2023) 100479.
[32] F.K. Yoshimoto, I.J. Jung, S. Goyal, E. Gonzalez, F.P. Guengerich, Isotope-labeling studies support the electrophilic compound I iron active species, FeO3+, for the carbon–carbon bond cleavage reaction of the cholesterol side-chain cleavage enzyme, cytochrome P450 11A1, J. Am. Chem. Soc. 138 (37) (2016) 12124–12141.
[33] S.A. Child, M.J. Reddish, S.M. Glass, M.H. Goldfarb, I.R. Barckhausen, F. P. Guengerich, Functional interactions of adrenodoxin with several human mitochondrial cytochrome P450 enzymes, Arch. Biochem. Biophys. 694 (2020) 108596.
[34] T. Omura, R. Sato, The carbon monoxide-binding pigment of liver microsomes. I. Evidence for its hemoprotein nature, J. Biol. Chem. 239 (7) (1964) 2370–2378.
[35] B. Schiffler, A. Zollner, R. Bernhardt, Stripping down the mitochondrial cholesterol hydroxylase system, a kinetics study, J. Biol. Chem. 279 (33) (2004) 34269–34276.
[36] H.M. Trang, D.E. Cole, L.A. Rubin, A. Pierratos, S. Siu, R. Vieth, Evidence that vitamin D3 increases serum 25-hydroxyvitamin D more efficiently than does vitamin D2, Am. J. Clin. Nutr. 68 (4) (1998) 854–858.
[37] J.E. Zerwekh, The measurement of vitamin D: analytical aspects, Ann. Clin. Biochem. 41 (Pt 4) (2004) 272–281.
[38] O. Klykov, B. Steigenberger, S. Pektas, D. Fasci, A.J.R. Heck, R.A. Scheltema, Efficient and robust proteome-wide approaches for cross-linking mass spectrometry, Nat. Protoc. 13 (12) (2018) 2964–2990.
[39] A. Chaikuad, C. Johansson, T. Krojer, W. Yue, C. Phillips, J. Bray, A. Pike, J. Muniz, M. Vollmar, J. Weigelt, Crystal structure of human ferredoxin-1 (FDX1) in complex with iron-sulfur cluster, Protein Data Bank 3P1M. Released (2010).
[40] J. Jumper, R. Evans, A. Pritzel, T. Green, M. Figurnov, O. Ronneberger, K. Tunyasuvunakool, R. Bates, A. Zidek, A. Potapenko, A. Bridgland, C. Meyer, S.A. A. Kohl, A.J. Ballard, A. Cowie, B. Romera-Paredes, S. Nikolov, R. Jain, J. Adler, T. Back, S. Petersen, D. Reiman, E. Clancy, M. Zielinski, M. Steinegger, M. Pacholska, T. Berghammer, S. Bodenstein, D. Silver, O. Vinyals, A.W. Senior, K. Kavukcuoglu, P. Kohli, D. Hassabis, Highly accurate protein structure prediction with AlphaFold, Nature 596 (7873) (2021) 583–589.
[41] M. Mirdita, K. Schutze, Y. Moriwaki, L. Heo, S. Ovchinnikov, M. Steinegger, ColabFold: making protein folding accessible to all, Nat. Methods 19 (6) (2022) 679–682.
[42] E.C. Meng, T.D. Goddard, E.F. Pettersen, G.S. Couch, Z.J. Pearson, J.H. Morris, T. E. Ferrin, UCSF ChimeraX: tools for structure building and analysis, Protein Sci. 32 (11) (2023) e4792.
[43] E.F. Pettersen, T.D. Goddard, C.C. Huang, E.C. Meng, G.S. Couch, T.I. Croll, J. H. Morris, T.E. Ferrin, UCSF ChimeraX: structure visualization for researchers, educators, and developers, Protein Sci. 30 (1) (2021) 70–82.
[44] G.C. van Zundert, M. Trellet, J. Schaarschmidt, Z. Kurkcuoglu, M. David, M. Verlato, A. Rosato, A.M. Bonvin, The DisVis and PowerFit web servers: explorative and integrative modeling of biomolecular complexes, J. Mol. Biol. 429 (3) (2017) 399–407.
[45] G.C. van Zundert, A.M. Bonvin, DisVis: quantifying and visualizing accessible interaction space of distance-restrained biomolecular complexes, Bioinformatics 31 (19) (2015) 3222–3224.
[46] R.V. Honorato, P.I. Koukos, B. Jimenez-Garcia, A. Tsaregorodtsev, M. Verlato, A. Giachetti, A. Rosato, A. Bonvin, Structural biology in the clouds: the WeNMR-EOSC ecosystem, Front. Mol. Biosci. 8 (2021) 729513.
[47] R.V. Honorato, M.E. Trellet, B. Jimenez-Garcia, J.J. Schaarschmidt, M. Giulini, V. Reys, P.I. Koukos, J. Rodrigues, E. Karaca, G.C.P. van Zundert, J. Roel-Touris, C. W. van Noort, Z. Jandova, A.S.J. Melquiond, A. Bonvin, The HADDOCK2.4 web server for integrative modeling of biomolecular complexes, Nat. Protoc. 19 (11) (2024) 3219–3241.
[48] K.A. Johnson, New standards for collecting and fitting steady state kinetic data, Beilstein J. Org. Chem. 15 (2019) 16–29.
[49] N. Mast, J.B. Lin, I.A. Pikuleva, Marketed drugs can inhibit cytochrome P450 27A1, a potential new target for breast cancer adjuvant therapy, Mol. Pharmacol. 88 (3) (2015) 428–436.
[50] E.C. Hulme, M.A. Trevethick, Ligand binding assays at equilibrium: validation and interpretation, Br. J. Pharmacol. 161 (6) (2010) 1219–1237.
[51] P. Hlavica, Mechanistic basis of electron transfer to cytochromes p450 by natural redox partners and artificial donor constructs, Adv. Exp. Med. Biol. 851 (2015) 247–297.
[52] F. Almarri, N. Haq, F.K. Alanazi, K. Mohsin, I.A. Alsarra, F.S. Aleanizy, F. Shakeel, Solubility and thermodynamic function of vitamin D3 in different mono solvents, J. Mol. Liq. 229 (2017) 477–481.
[53] STREDNA ID LNJNJW, LNJNJW, 2025, https://doi.org/10.22011/strenda_db.
[54] E.O. Yablokov, T.A. Sushko, P.V. Ershov, A.V. Florinskaya, O.V. Gnedenko, T. V. Shkel, I.P. Grabovec, N.V. Strushkevich, L.A. Kaluzhskiy, S.A. Usanov, A. A. Gilep, A.S. Ivanov, A large-scale comparative analysis of affinity, thermodynamics and functional characteristics of twelve cytochrome P450 isoforms and their redox partners, Biochimie 162 (2019) 156–166.
[55] N. Jay, J.E. McGlohon, D.F. Estrada, Interactions of human mitochondrial Ferredoxin 1 (Adrenodoxin) by NMR; modulation by cytochrome P450 substrate and by truncation of the C-terminal tail, J. Inorg. Biochem. 249 (2023) 112370.
[56] C.D. Charvet, J. Laird, Y. Xu, R.G. Salomon, I.A. Pikuleva, Posttranslational modification by an isolevuglandin diminishes activity of the mitochondrial cytochrome P450 27A1, J. Lipid Res. 54 (5) (2013) 1421–1429.
[57] J.E. McGlohon, J. Logothetis, D.F. Estrada, NMR-guided identification of CYP11A1-Adrenodoxin interactions that differentially govern cholesterol and vitamin D3 metabolism, J. Biol. Chem. 301 (8) (2025) 110428.
[58] N. Sawada, T. Sakaki, M. Ohta, K. Inouye, Metabolism of vitamin D_3 by human CYP27A1, Biochem. Biophys. Res. Commun. 273 (3) (2000) 977–984.
[59] D.A. Murtazina, U. Andersson, I.S. Hahn, I. Bjorkhem, G.A. Ansari, I.A. Pikuleva, Phospholipids modify substrate binding and enzyme activity of human cytochrome P450 27A1, J. Lipid Res. 45 (12) (2004) 2345–2353.
[60] H.M. Peng, C. Barlow, R.J. Auchus, Catalytic modulation of human cytochromes P450 17A1 and P450 11B2 by phospholipid, J. Steroid Biochem. Mol. Biol. 181 (2018) 63–72.